Magnetic Archaeology

Executive Summary

Individual LENRs are believed to deposit energy locally and quickly, only affecting a small volume (~ 100 nm in size) for a very short time (~ 1 psec) before the energy dissipates into the surrounding material. Detecting temperature rises, at unknown space-time locations, with either this temporal or this spatial resolution is challenging enough; doing both simultaneously is well beyond our current capabilities.

In principle, thermal history recorders offer us an attractive way to reduce this dimensionality; they'll tell us whether or not an event has occurred at a given site, but not when it did so. This is a tradeoff well worth taking. However, there is one caveat; to be useful for LENR detection, the "recorder" must be quick enough to respond on psec timescales; otherwise LENR events will be washed out and missed. Conventional history recorders, such as thermal paints or phase change materials rely on chemical reactions or atomic motion, and are far too slow to detect psec-scale events. However, magnetic effects, being based on electron spins, occur much faster, and will respond on sub-psec timescales. Accordingly, we have developed magnetically-based thermal history recorders, and used them in our magnetic archaeology campaign to try to detect LENR.

Single domain, nanoscale magnets have been used for decades in the data storage industry as a method for storing information in a non-volatile medium. The information is saved to memory by flipping or reorienting the natural magnetic polarity of a local metallic film structure, domain, that can later be read back effectively as a 0 or 1. The magnetic fields are normally very stable, and can persist for years. However, the nanomagnets can become destabilized from 1 to 0 if locally heated to a high enough temperature. This thermal-destabilizing effect, responsive to local heat input, is what made this method of detection truly attractive for detecting LENR events. At these length scales and the temperature requirements for a magnet to flip, we were able to form nano sized dots (≤200 nm) that could detect a single 24 MeV D-D event within a few 100 nm of its center. With Pd films adhered in close proximity to these sensors we have not observed any observable quantities of heat that can be attributed to anomalous heat events (AHE) or low energy nuclear reactions occurring in the Pd lattice. Methods implemented here were focused on magnetic sensor design and read-out of magnetic signals from these sensors making sure to maximize signal to noise in both magnetic polarity resolution and spatial resolution. FePt alloy films were developed for nanodot sensors, and magnetic force microscopy (MFM) as well as scanning tunnel magneto resistance (TMR) were used as sensor readouts.

Background

The fundamental mechanism magnetic archaeology is based around, is that the alignment of magnet dipole moments becomes disordered at elevated temperatures, at which point they are susceptible to outside magnetic field influence. A hard magnetic material is generally understood to possess high remanent magnetization (M_R), meaning in the absence of large externally applied fields (H) it retains a relatively large density of magnetic dipole moments that are oriented along a single vector, compared to the density at full saturation (M_S). Hard magnets also require larger coercive H fields to flip the orientation of these dipoles from vector $\hat{\imath}$ to $-\hat{\imath}$. This is depicted through its coercivity, H_C. At increased temperatures both M_R and H_C typically decrease, and at a critical temperature, referred to as the Curie Temperature (T_{Curie}), these values are reduced to 0 where there

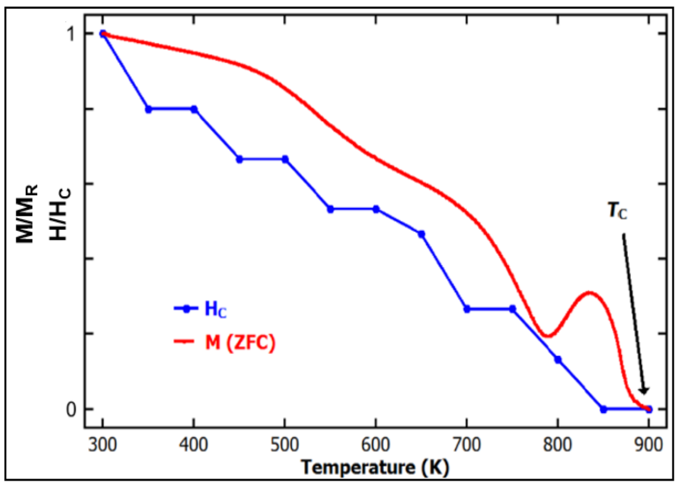

Figure 1: Thermo-magnetic plot of the coercive field strength (blue), normalized to the room temperature value, indicating switching field requirements. Zero-field-cooled (ZFC) thermos-magnetization plot (red; $\mu_0 H = 0.01$ T), also normalized to its room temperature value, indicating a Curie temperature of TC < 900 K.[1]

is no measurable long range magnetic order. This loss of magnetic order persists while the material remains above T_{Curie}, but upon cooling, the polarity of each atom can still be reoriented if exposed to an external magnetic field.

Understanding and applying this basic principle above, people have been able to store information through magnetic polarity vectors pointing up or down on a 2D matrix of nanodomain structures. As mentioned in the summary, this phenomenon has been extensively applied and optimized for non-volatile memory storage in computer hard disk drives (HDDs). A hard magnetic thin film that contains trillions of nanodomains (bits) on the surface are polarized up or down (0 or 1) using a magnetic write head that scans across the surface applying brief but high intensity magnetic fields localized to <100 nm. Standard hard drives utilize perpendicular magnetic recording (PMR) where the vectors point out of the platen plane. State-of-the-art hard drives use heat-assisted magnetic recording (HAMR) methods to (1) decrease writing field needed to flip a domain, (2) increase domain or bit stability at room temperature, (3) and further decrease size of the domain size (<10 nm) increasing memory density >1Tb/in^2). The stability of a domain with respect to temperature is inversely proportional to the domain's coercivity and magnetization (Figure 1[69]).

The complexity of the film stack in HDD substrates or platens is more complicated than just having a single hard magnetic layer on top of a rigid glass substrate. In Figure 2 it can be understood that there are ≥7 layers that each contribute to the writability, bit stability, and scratch/corrosion protection of the hard magnetic film. For the purposes of this report please refer to more detailed literature that explains form and function of PMR HDD technology[70,71].

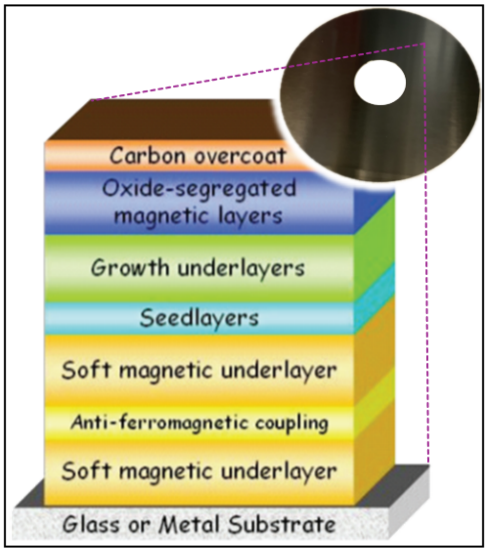

Figure 2: Traditional film stack to support reading and writing patterned magnetic media. The layers in green, lightt blue and yellow are to assist in bit stability, grain orientation, and signal enhancement for read-out. The dark blue layer is the film that actualy stores information in a hard magnetic material.

The ability for local heat sources to be able to distort and destabilize the magnetic structure of a magnet makes these material systems very useful for detecting AHE in Pd thin films, nanoparticles, and other Pd form factors that have at least one dimension reduced to the micro/nanoscale. It can effectively record a thermal event with high spatial accuracy that we can then read back using techniques that detect magnetic field, fluxes, or gradients. Literature has shown magnetic structure can be changed at picosecond and femtosecond timescales when using lasers as the pump and/or probe[72,73,74]. Since the thermal effects from D-D fusion type nuclear events may persist for

---

[69] Scheunert, G.; Cohen, S. R.; Kullock, R.; McCarron, R.; Rechev, K.; Kaplan-Ashiri, I.; Bitton, O.; Dawson, P.; Hecht, B.; Oron, D. Beilstein J. Nanotechnol. 2017.
[70] Kane, Margaret M. "Fabrication and characterization of perpendicular magnetic anisotropy thin-film CoCrPt grown on a Ti underlayer". 2015.
[71] Dong, Y., "Micromagnetic Study of Perpendicular Magnetic Recording Media", PhDT, 2012.
[72] Proenca, M.P., Muñoz, M., Villaverde, I. *et al.* Deterministic and time resolved thermo-magnetic switching in a nickel nanowire. *Sci Rep* **9**, 17339 (2019).
[73] Vahaplar, K et al. "Ultrafast path for optical magnetization reversal via a strongly nonequilibrium state." *Physical review letters* vol. 103,11 (2009).
[74] Hirofumi Suto, Akira Kikitsu, Yoshinori Kotani, Tomoyuki Maeda, Kentaro Toyoki, Hitoshi Osawa, Nobuaki Kikuchi, Satoshi Okamoto, Tetsuya Nakamura; Time-resolved imaging of an operating hard-disk-drive write head using nano-beam x-ray magnetic circular dichroism. *J. Appl. Phys.* 7 October 2020.

picosecond or longer timescales, these materials as magnetic sensors should have more than enough time resolution to capture an event that occurs in close proximity. Furthermore, since the read-out method only needs to measure changes in magnetic field direction and/or amplitude, this method of detection does not require permanent film damage (Pd or sensor) for the user to detect if a thermal event/reaction occurred! Changes in magnetic structure do not necessitate physical changes to the lattice structure. This is crucial in data reliability, repeatability, and reproducibility between sample to sample and experiment to experiment. We do not need to be as careful with surface cleanliness and local debris prior to an experiment since most debris will not have a magnetic signature and remain invisible.

The sequence of events of how a magnetic domain would record an AHE event is depicted in Figure 3. We first magnetize all domains in a single direction, e.g., "North" (pointing out of the surface), using a magnetizer set to pulse a 4 Tesla field through the film. Once the Pd film is loaded under ultrapressure conditions the stimulation pulse, either through Joule heating or laser absorption, would stimulate the Pd up to a threshold temperature that is still below the switching temperature (T_S) for the magnetic domains for a given external field (H_{ext}) amplitude. If an LENR-related thermal event occurs this would further increase the temperature of the Pd, and by conduction the magnetic sensor, above T_S, switching local domains in the direction of H_{ext}. After

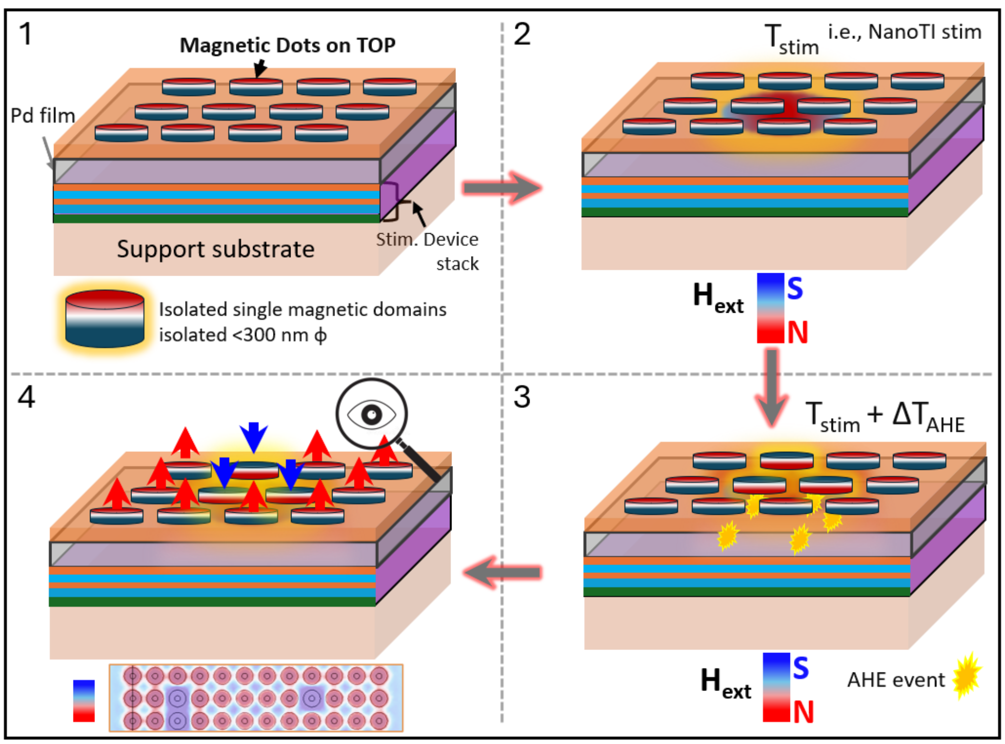

Figure 3: a)All spatially isolated single domains are mangetized in one direction in a preconditoned state. b) The Pd is thermally stimulated from external source to below a switching threshold temperature. c) If AHE forms locally the additonal input energy will increase the dots temperature enough to flip the domain orientation to the direction of the applied H field. d) post inspection of themagnetic signal for each domain is carried out to see if domains were altered during the course of the experiment.

the system cools back down to room temperature (within μs→ ms) the switched domains now persist within the film structure, and their magnetic fields can be read out in post experiment characterization to confirm existence of local LENR.

The main drawbacks to this detection method are that we are currently limited to thin films, and we cannot know, in real time, at what point in an experiment a thermal event occurs, we can only know if it did or did not occur *ex-situ* with high spatial sensitivity.

The methods used to read or scan the surface of each sample, magnetic force microscopy and tunneling magnetoresistance, will be discussed further in the methods section. However, the reasoning for selecting these two methods of magnetic detection came down to spatial resolution, ease of implementation, and ability to scan quickly over 100s of microns while maintaining high fidelity. The magnetic force microscopy (MFM) technique is a proven tool for qualitatively measuring changes in emitted fields from the surface of a material, in this case a planar film. This technique allows for scanning at high spatial resolution, but at modestly small scanning arrays <50x50 μm^2. Tunneling magnetoresistance (TMR) microscopy allows for a quantitative readout of resistance changes in a sensor's circuit from changes in local fields making it more robust. This technique, which is used by read heads in commercial hard disk drives (HDDs), required significant design and prototype work though, since high spatial resolution TMR sensors are optimized for steady, non-contact, uni-directional scanning inside an HDD, not the bi-directional, surface-contact, raster scanning used in our application.

Methods

Methods : Detecting magnetic polarity

Given the thin film morphology for these magnetic materials, the domains that are polarized up or down have exceedingly small domain volumes with emitted field (*B*) decaying as a function of inverse distance cubed from the center of the domain (*Equation 1*). First principle magnetic simulations at the micro and nanoscale indicate that >99 % of the magnetic field intensity is lost at ≥1 µm gap away from the thin film surface to the read-out probe that is measuring the field (Figure 4). This necessitates the requirement that our read-out method for AHE magnetic sensors

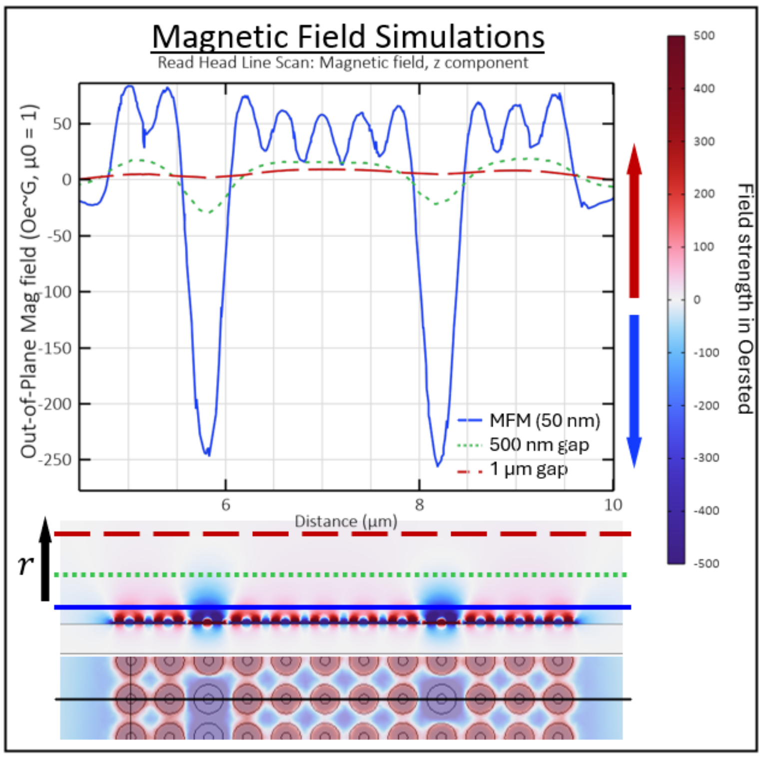

*Figure 4: COMSOL permanent magnet simulation. Blue, green, and red scans plotted are line scans from a probe at a set distance **r** from the magnetic domain surface. Y axis indicates the magnitude and sign of the emitted field strength. Domains are polarized up or down from the film surface (50 nm- 1 µm).*

must be able to probe the emitted fields <<1 µm away from the film surface to maintain a high signal to noise ratio.

Equation 1 $$B = \frac{\mu_0 I A\sqrt{1+\cos^2(\theta)}}{4\pi r^3}$$

1: Polar Magneto Optical Kerr Effect (MOKE) Microscopy

This technique takes advantage of changes in photon incident and reflected angles off a magnetic material surface. Using a polarized ultraviolet light source, the Kerr rotation of the polarized light can be captured over the entire focal plane making it an ideal technique for obtaining magnetic data over large surface areas in a short period of time[75,76]. The contrast can be enhanced taking the differential between 2 images of positive and negative angle polarizer rotation, increasing contrast between domains that have opposite magnetic polarity[77]. The Kerr rotation is directly related to the sign and amplitude of the local magnetic field the light interacts with, as its irradiance drops exponentially under the surface. The great advantage for this technique is that it is able to quickly obtain magnetic polarity or moment maps of the sample surface over 100s µm in a single image. An example of a polar MOKE image is in Figure 5 from a credit card magnetic strip. However, this technique was ultimately not implemented in our experimental approach for magnetic characterization and analysis due to fundamental optical limitations in lateral resolution based off the Rayleigh criterion for available 450 nm wavelength sources and 50x objective lens. This means we would not be able to reliably resolve <500 nm magnetic features with high confidence.

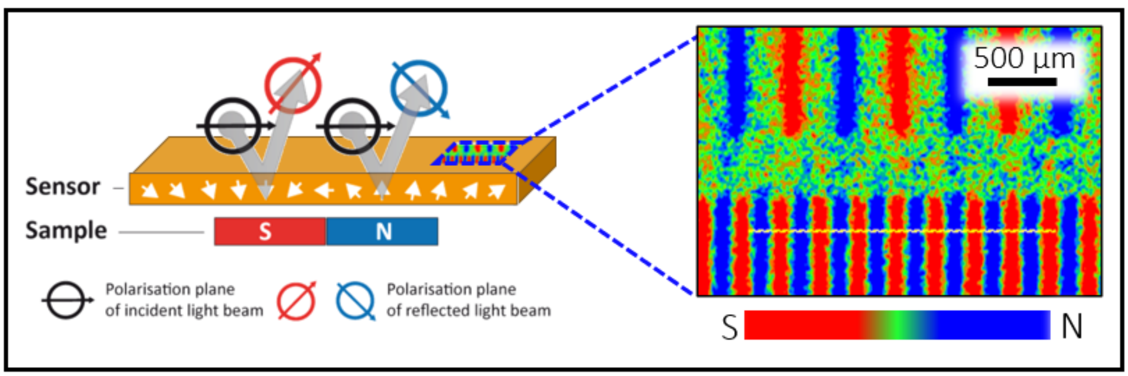

Figure 5: When the MOKE sensor is in close proximity to the sample surface the soft magnet in the MOKE sensor reorients to align with the moment polarity in the sample. A polarized light is reflected off the back of the sensor film being rotated slightly in the local orientation of the magnetic field upon reflection (left). The incident and reflected signals are differentiated to produce the blue to red color gradient image (right). Image is a magnetic strip.

---

[75] Jeffrey McCord 2015 *J. Phys. D: Appl. Phys.* **48** 333001.

[76] M. Takezawa, K. Maruko, N. Tani, Y. Morimoto, J. Yamasaki, T. Nishiuchi, S. Hirosawa; Magnetic domain observation of hydrogenation disproportionation desorption recombination processed Nd–Fe–B powder with a high-resolution Kerr microscope using ultraviolet light. *J. Appl. Phys.* 1 May 2010; 107 (9): 09A724.

[77] H. Z. Yang, Y. J. Chen, S. H. Leong, C. W. An, K. D. Ye, M. J. Yin, J. F. Hu; A multi-functional testing instrument for heat assisted magnetic recording media. *J. Appl. Phys.* 7 May 2014; 115 (17): 17B726.

2: Magnetic Force Microscopy (MFM)

MFM is a technique that operates identical to a traditional AFM that scans across the surface of a sample, usually moving in a serpentine path. The atomically sharp tip (≤80 nm radius) is coated with a thin layer of CoCr which is traditionally defined to have medium/hard magnetic properties. The tip is polarized parallel to the tip axis, so the CoCr domains have a polarity pointing up or down when the cantilever is mounted into the AFM chassis and therefore is most sensitive to out-of-plane stray magnetic fields. When the tip is near a local magnetic field with high magnetization it will deflect and change the phase of the resonant frequency of the cantilever depending on the polarity of the stray field (Figure 6). MFM typically requires 2 scans across the same line path. For this project, the first pass scans the surface topography in AC tapping mode, the second (also called a nap scan) lifts the tip above the surface so the amplitude and phase of the resonant frequency are only influenced by external magnetic fields or local charges, not topography. The charge effects are mitigating by grounding the tip and sample to a common ground. This allows us to obtain both topography and magnetic contrast over the same sample surface area at <10 nm resolution (Figure 7 and Figure 8)[78].

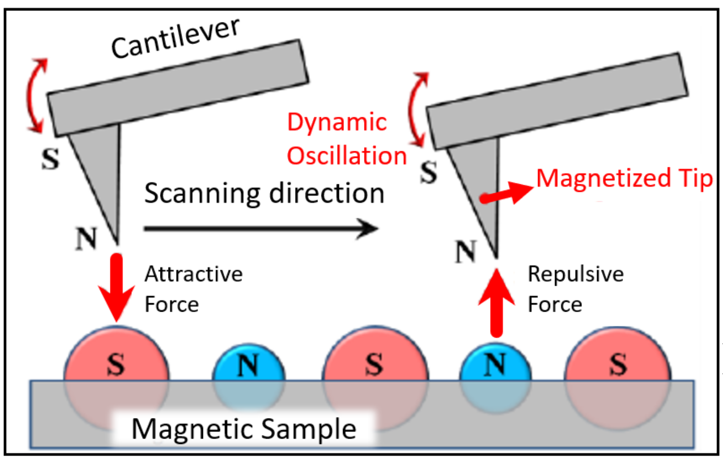

Figure 6: Pictorial diagram of how the AFM-MFM tip interacts with a magnetic surface with local variation in North or South magnetic polarization.

For this research all MFM scans are set-up so that an increase in phase angle indicates a sample domain is polarized north (field out of the surface) and a decrease in phase angle means the domain is polarized south (field into the surface). This method is inherently slow, being limited to small scan areas to maintain exceptional spatial fidelity, and without calibration is a qualitative measurement for magnetic polarity only, north or south. In detecting AHE, we only need the north or south polarity information and not necessarily the amplitude. This technique was the main

[78] T. Bublat, D. Goll; Influence of dot size and annealing on the magnetic properties of large-area L1-FePt nanopatterns. *J. Appl. Phys.* 1 October 2011.

diagnostic used for measuring magnetic polarity in all sample types through the course of magnetic archaeology projects.

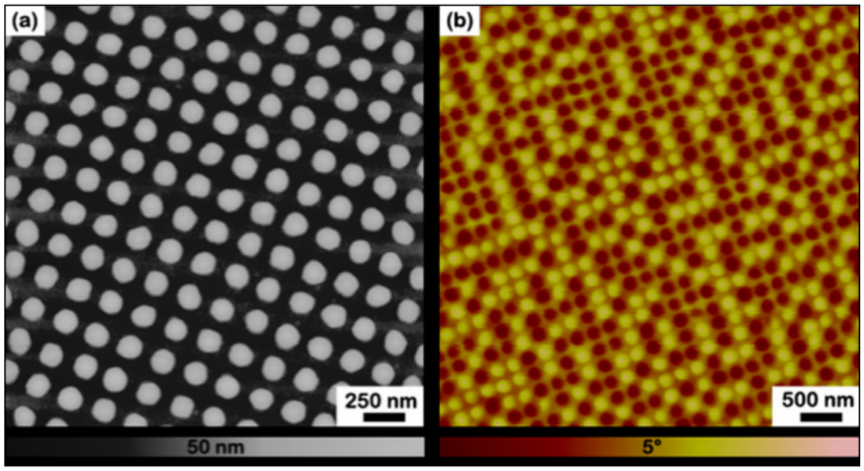

Figure 7: a) Topography image from first scan, AC tapping mode of magnetic dot features. b) MFM phase contrast on the nap scan showing each dot contains a single domain oriented up or down with repect to the sample surface.

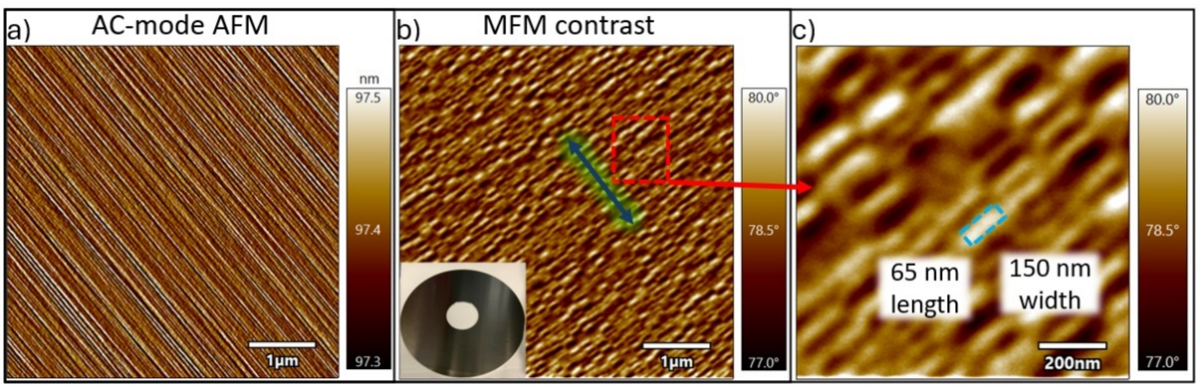

Figure 8: AFM scan of HDD platen used in our chips as starter substrates. a) topography scan showing low roughness striations from the read/write head arm. b,c) MFM contrast scan showing "racetrack" of magnetic bits along the write head path.

Image Analysis Pipeline

To speed up the analysis process for comparing pre and post experiment MFM magnetic polarity scans for each individual dot/magnetic domain on samples with >10,000 dots, an image filter software pipeline was developed to automate this visual process. The program located each dot within the MFM scan as seen in Figure 9a by first looking at the topography image collected at the same time and location the MFM contrast data is collected. An edge detection module is employed to locate the edges of all dots in the image based off sharp gradient changes in pixel intensity. With the location of each dot or region of interest (ROI) logged, ROIs are then mapped directly onto the MFM scan, Figure 9c. Depending on the threshold values for pixel area and average pixel intensity, set by the user, the ROI for each dot is filtered as having either North (red) or South (blue) polarity.

We also accounted for physically missing dots in the array and negated the polarity information in the MFM scan for that area, leaving a white space in the final area map.

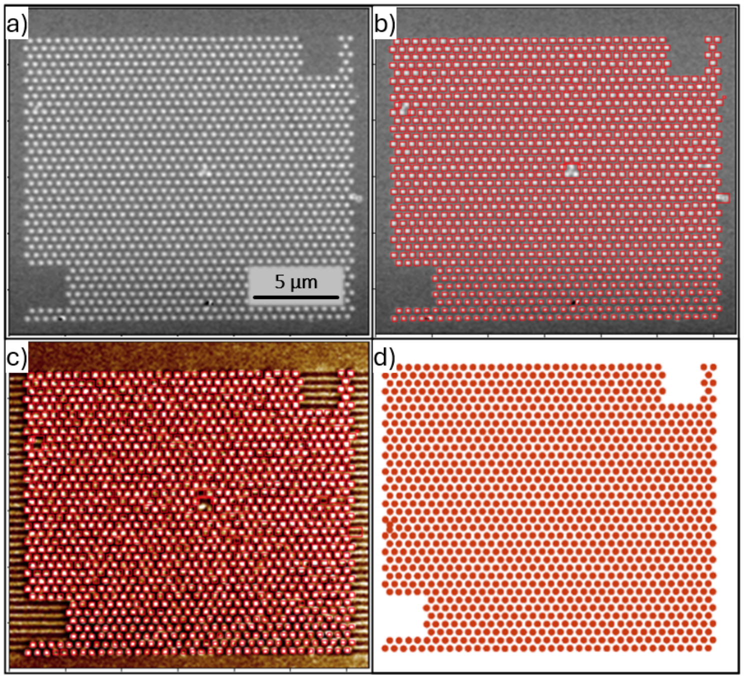

Figure 9: a) Topography scan used for initial map for located physical coordinates for each dot feature in the array. b) Resulting ROI boxes outline boundaries for each dot. c) ROIs from b) mapped to the MFM scan where the pixel intensity within each ROI are averaged and normalized to background pixel intensity (a dark brown shade). d) based on pixel intensity thresholds each dot is measured to be either oriented North (red) or South (blue). In this case this array is in a preconditioned state of all North polarized domains.

3: Tunneling Magnetoresistance (TMR) Microscopy

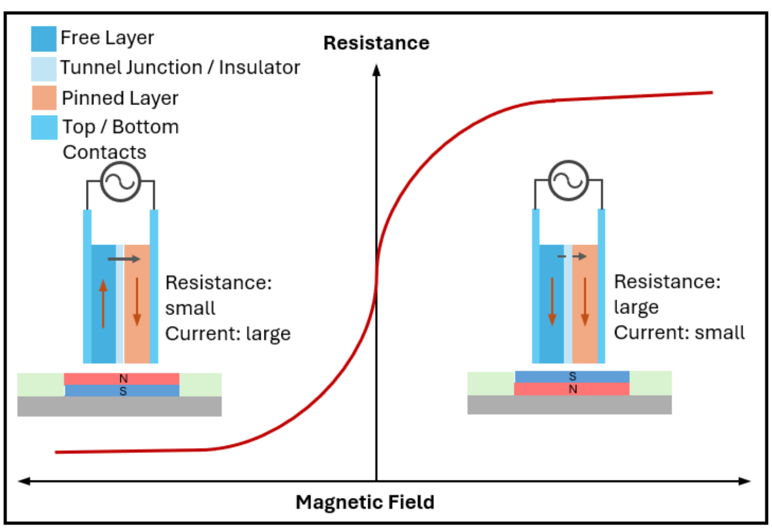

Figure 10: Resistance change of a TMR circuit as a function of local magnetic field change from north to south until the tunnel junction is saturated.

The last method of read-out used for measuring our samples is TMR which exploits a magnetoresistive effect that occurs in a magnetic tunnel junction with an ultrathin insulating layer[79]. One side of the junction is pinned to have a magnetic orientation that does not change while the free layer can be flipped in orientation to be parallel or antiparallel by local external fields of an HDD or magnetic sample in general[80,81]. Measured sensor resistance is dependent on the local magnetic field of a sample surface and is a quantitative measurement of the local magnetic vector down to a spatial resolution of roughly 50 nm and dependent on the physical dimensions of the TMR junction (Figure 10). This technology is used in read heads of hard drives to achieve high storage densities and has been optimized for flying over an HDD platen spinning at >5000 rpm on what is called a slider; billions of dollars have been gainfully invested in this development. However, the samples for AHE experiments could not be easily scanned by high-speed rotation and therefore we needed to design our own in-house TMR microscope that could scan selective areas of a sample with a resolution requirement of ≤100 nm.

To solve this problem, TMR read heads were salvaged from existing HDD units and operated using an AC voltage driven source. Data read out was done by monitoring variation in current across the tunnel junction and calculating the change of resistance. Two off-axis optical microscopes were used to locate the sample alignment marks while nanometer resolution, single axis x, y, and z piezo motors were used to drive the sample position underneath the TMR read head with sub 5 nm precision (Figure 11). A more detailed set of SEM images are in Figure 12 showing the actual tunneling junction. An example TMR scan can be seen in Figure 13 for a sample containing 300

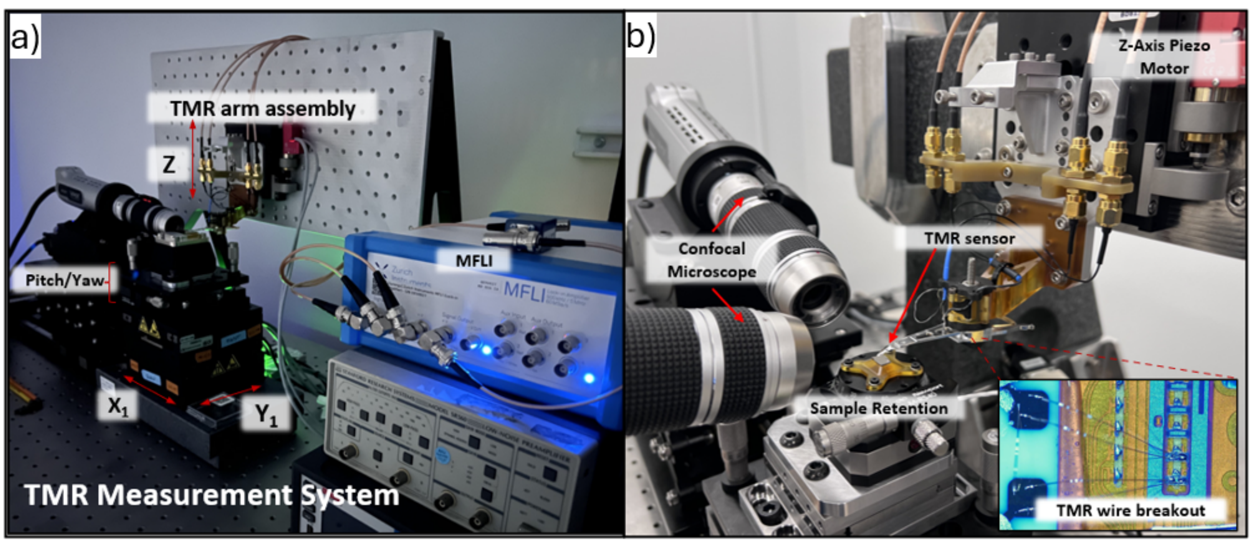

Figure 11: a) TMR apparatus overview. TMR assembly contains the read head details in the next figure. b) close-up image of off-axis confocal optical microscopes pointed at sample surface to align sample fiducials. Detail view shows the custom wire bonding required to interface with and control the read head sensor that was harvested from the HDD.

---

79 Zhang, X., Butler, W. (2016). Theory of Giant Magnetoresistance and Tunneling Magnetoresistance. In: Xu, Y., Awschalom, D., Nitta, J. (eds) Handbook of Spintronics. Springer, Dordrecht.

80 D. Mitin, M. Grobis, M. Albrecht; Scanning magnetoresistive microscopy: An advanced characterization tool for magnetic nanosystems. *Rev. Sci. Instrum.* 1 February 2016; 87 (2): 023703.

81 Nakatani T, Gao Z, Hono K. Read sensor technology for ultrahigh density magnetic recording. MRS Bulletin. 2018;43(2):106-111.

nm FePt dots having all their polarities oriented in the same direction. The dots appear elongated due to slight drift in the motor positions during the time it takes to complete one scan. Unfortunately, this measurement technique was never deployed for measuring actual AHE samples due to the project being wrapped up prior to full TMR readiness.

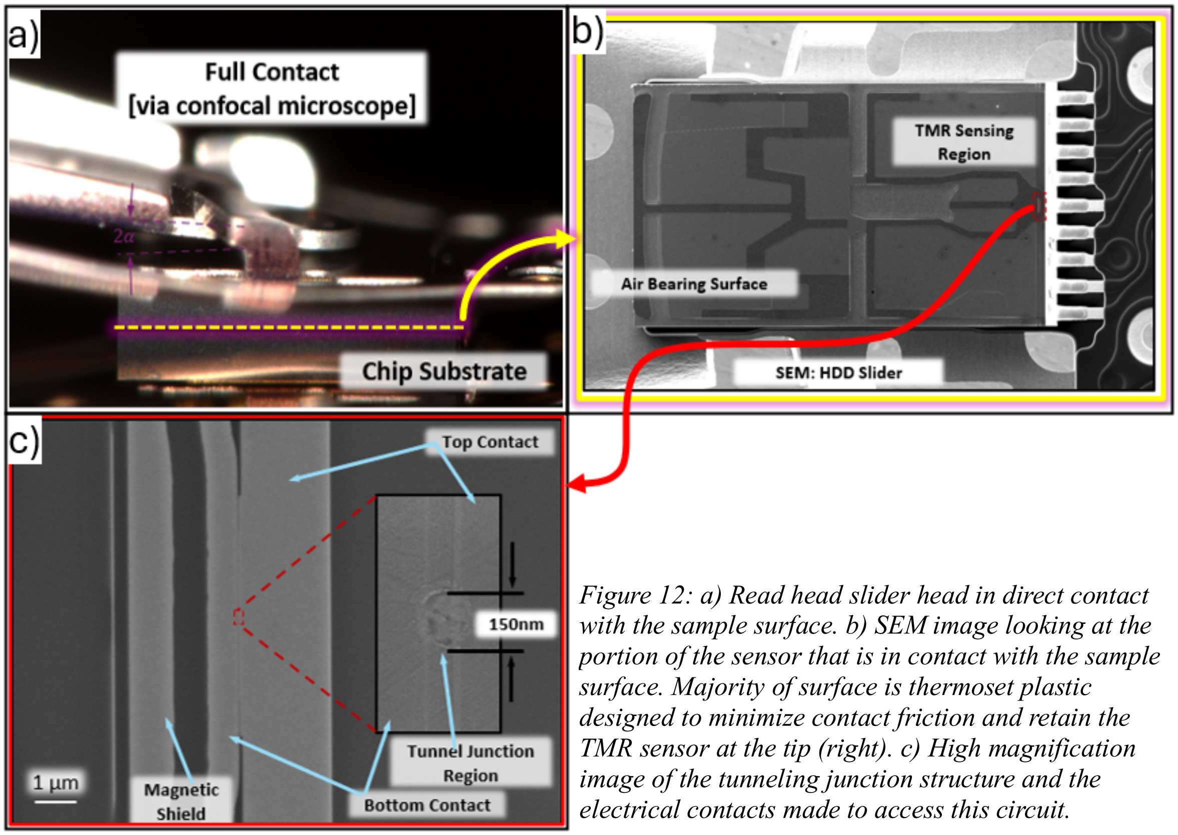

Figure 12: a) Read head slider head in direct contact with the sample surface. b) SEM image looking at the portion of the sensor that is in contact with the sample surface. Majority of surface is thermoset plastic designed to minimize contact friction and retain the TMR sensor at the tip (right). c) High magnification image of the tunneling junction structure and the electrical contacts made to access this circuit.

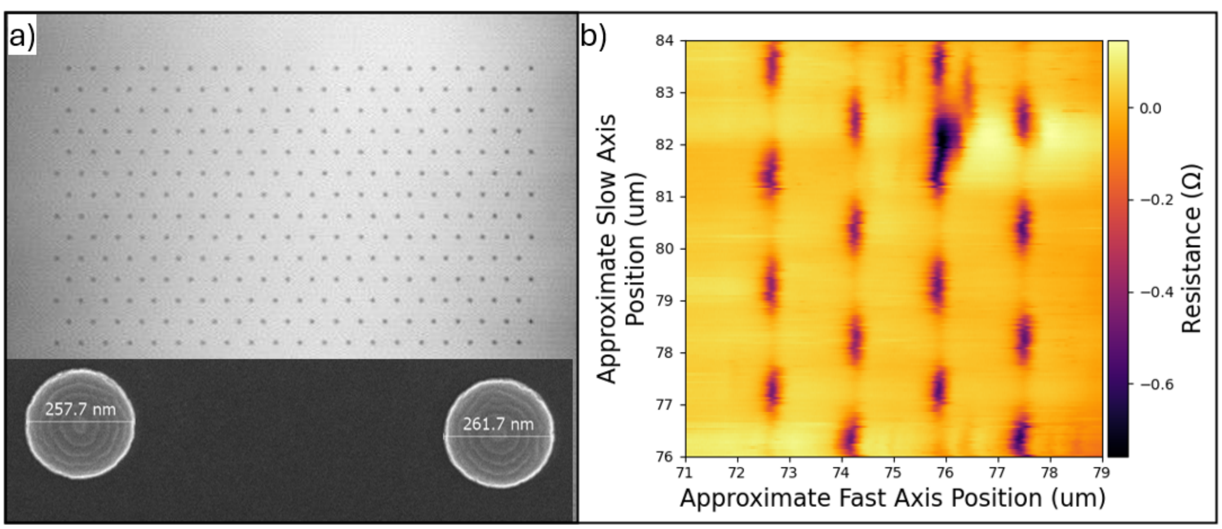

Figure 13: a) SEM image and high magnification image of 250-300 nm dots scanned by TMR system. b) TMR resistance-change read out over an 8x8 µm area. The dots were polarized in a Northward polarity indicated by a decrease in resistance. The dots are elongated in the slow axis due to small drift in the piezo motor position over the course of the scan.

Methods : Fabricating Samples

Materials selection for the magnetic AHE sensor was based off multiple requirements that were chosen to maximize phase stability (temperature and chemical), minimize susceptibility to sensor degradation from handling and extraneous fields, and minimize complexity of film architecture. Selection criteria are listed below.

1. High coercivity (H_C) at room temperature (>5 kOe) up to 200 °C
2. Curie temperature (T_C) variable between 350-900°C
3. Single domain size with high magnetocrystalline and shape anisotropy down to 50 nm
4. Out-of-plane magnetization with magnetic easy axis aligned perpendicular to substrate surface
5. Minimal reactivity to hydrogen gas
6. High remanent magnetization (M_R) flux density for bit stability both *in situ* and *ex situ*
7. Can be lithographically patterned, etched, and coated while maintaining compositional and phase integrity

The two material systems chosen were CoPtCr and FePt. Both have extensive literature in memory applications, and therefore have a good track record of fulfilling criterion 1-4. Internal tests were completed to confirm or deny the last 3 requirements essential for these magnetic archaeology tests.

1: CoPtCr- Standard for PMR in HDD platens

Instead of ourselves synthesizing the ternary phase film structure of magnetic CoPtCr using complex sputtering processes and exotic metallic seed layers, initial magnetic archaeology magnetic sensors utilized the existing film architecture in HDDs that can be purchased off the shelf. The HDDs contain between 2-6 platens that are glass substrates coated with CoPtCr films ready to be used in storage applications. The general film stack is seen in Figure 14 where you can see the complexity of this technology which has already been optimized for this specific industry. Purchasing allowed us to cheaply obtain many HDD platens with effectively <100 nm domain sensors within days instead of months. Subjecting these platens to ultrapressure hydrogen conditions sooner rather than later in the project helped in affirming our hypothesis that these films were robust in these harsh environments at an early stage of development. It is important to clarify here, that ultimately for the final iterations of sample development in this project, we moved away from using HDD platens as the material for magnetic sensing. This was due to issues with repeated delamination, increased complexity of reading out the magnetic signature of this film, low Curie temperature (~150 °C), and low amplitude of M_R signal making it a noisy dataset to filter and analyze. However, as an initial, rapidly implementable, approach it was a useful step to take.

Experimental chips were fabricated using these platens as substrates. Chips for both NanoTI and Staring type AHE experiments were designed, fabricated, and tested with the CoPtCr sensor being buried underneath a layer of gas-loadable Pd. Due to the bulk service temperature limit of these platens roughly set at 150 °C all fabrication processes needed to minimize substrate heating to below 140 °C so as to not degrade the complex layer structure. The HDD platens firstly need to have the diamond like carbon (DLC) coating removed using a diamond/oxide etch clean, the DLC coating made the surface hydrophilic making it difficult to spin coat positive photoresist for further pattern development.

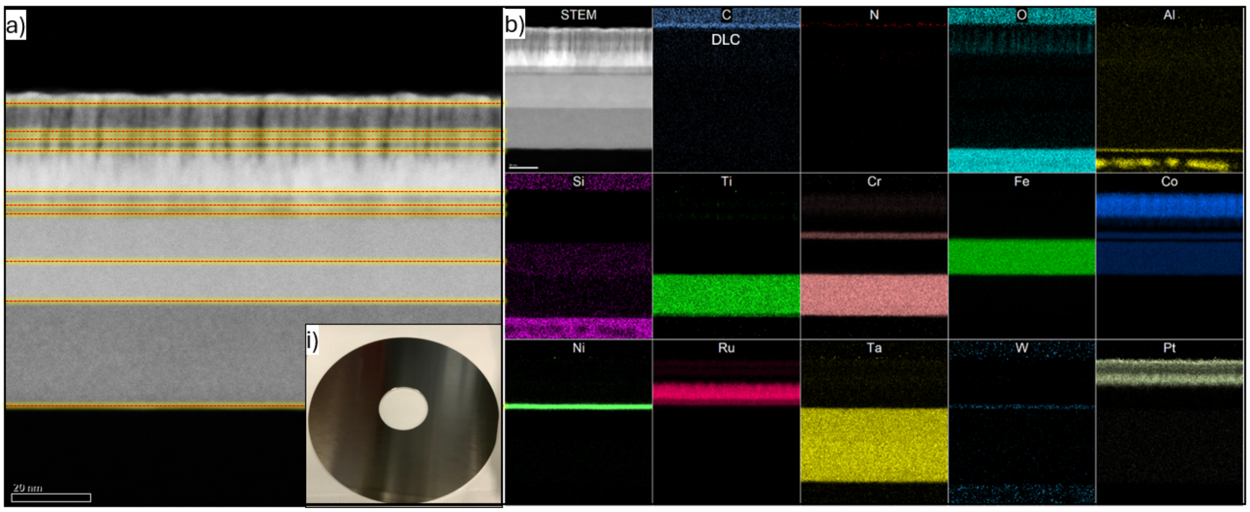

Figure 14: a) FIB lamella cross section imaged with STEM showing individual layers of the top 75 nm from the surface of an HDD platen. Below these layers is a SiO_2 based substrate up to 500 µm thick. There are >10 layers in this architecture. B) STEM-EDS maps of the same cross-section area in a). Each color indicating a specific element called out for each sub-image. The applications for each layer are similar to the general overview structure displayed in the concept section.

2: **CoPtCr – Staring Chips**

After DLC removal, 50 nm Pt markers were deposited using e-beam evaporation with a 5 nm Cr adhesion layer. 50 nm of SiO_2 acted as a passivation layer between the CoPtCr and Pd sample that is placed on top to prevent unwanted alloying and possible interference with the CoPtCr crystalline structure. It also slowed diffusion of protium or deuterium reaching the magnetic layer during a test. Plasma enhanced chemical vapor deposition (PECVD) was used for all dielectrics, including

SiO_2, for these chips. Finally, 50 nm Pd was patterned on top with 5 nm Cr adhesion layer allowing for unimpeded gas loading at the Pd surface (Figure 15).

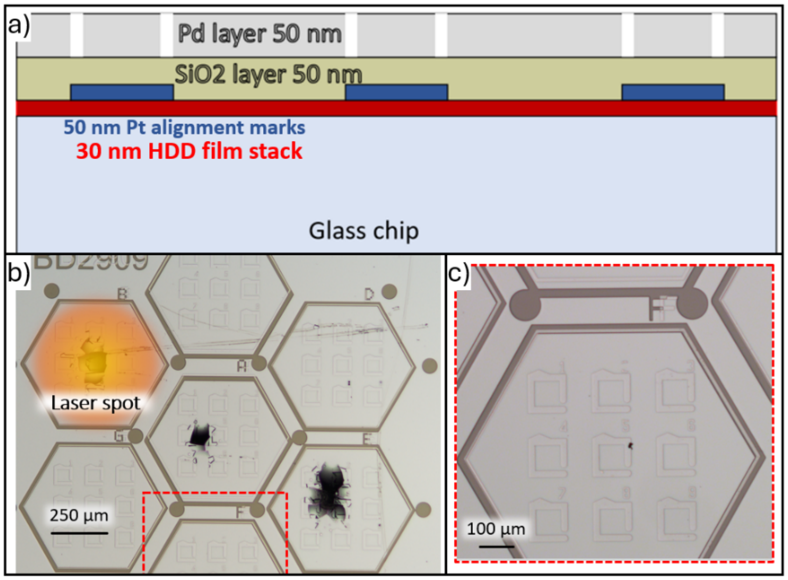

Figure 15: a) Chip cross-section in L-edit software showing multi-layer film structure. Pd is on top to ensure loading and direction absorption of laser power from Staring laser. b) Example top-down view of the HDD staring chip with stim pads A,B, and F damaged from laser shots. c) Higher magnification of individual laser stim pad with 9 sub-boxes (100x100 µm). These boxes are used to locate the MFM and or TMR sensors over the ROI prior to starting a pre or post scan for magnetic read-out.

3: **CoPtCr – NanoTI Chips**

The additional film stack for these chips used in the NanoTI experimental campaign are similar to the architecture used in the non-magnetic-archaeology chips used in NanoTI. For more detail on the methodology of how the chip operated for thermal coefficient calibrations and AHE experiments please refer to the Chips campaign section of this report. Chip fabrication for magnetic archaeology followed the film stack in Table 1. Up to eight 20 x 20 µm Pt serpentine heater devices, to provide resistive stimulation during the experiments, were patterned onto a single chip to account for lower device yield and shorter experimental turnaround times (Figure 16). Various sizes of Pd targets were made between 5-30 µm square to vary the peak temperature and thermal gradients reached for each target, stimulated at the same current and voltage parameters. Pulse widths for stimulation varied between 5-20 µs with 5-25% duty cycle.

Table 1: HDD -Thermal Arch NanoTI Fabrication Steps

Step #	Material	Method	Feature
1	5 nm Cr/ 50 nm Pt	E-beam Evap	Alignment marks
2	20 nm SiO_2	PECVD	Passivation
3	5 nm Cr/100 nm Pd	E-beam Evap	Pd target
4	100 nm SiO_2	Oxide Etcher (ICP)	Passivation/loading windows for Pd
5	5 nm Cr/ 100 nm NiCr	E-beam Evap	Pt heater/RTD
6	10 nm Cr/200 nm Au	E-beam Evap or Sputter	Interconnects/Contacts

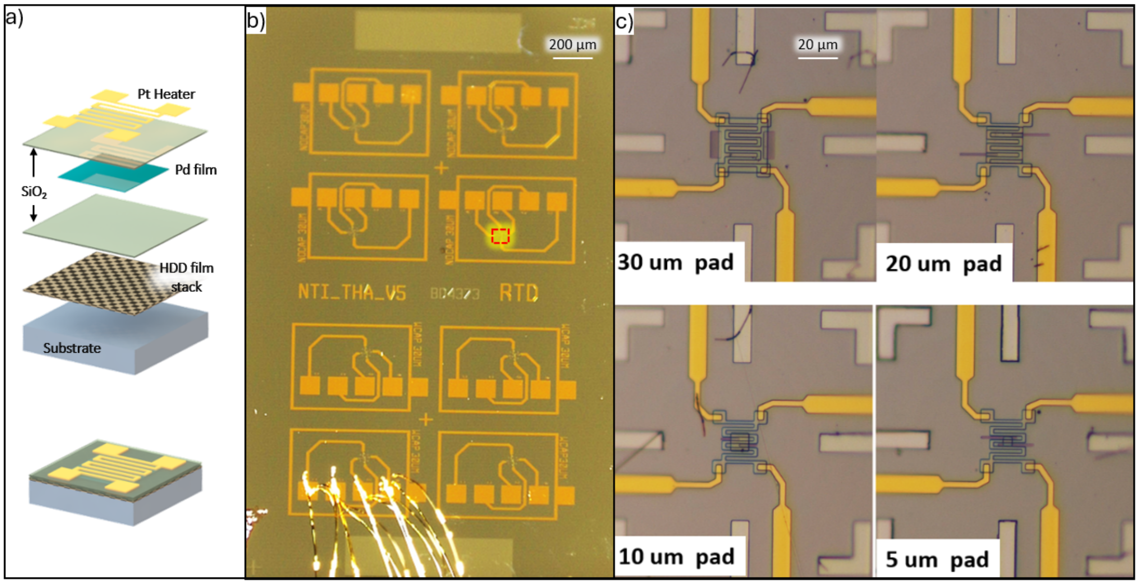

Figure 16: a) Exploded view of film stack used in HDD NanoTI type chip architecture. b) Top-down view of chip with 8 stimulation circuits with one wire-bonded to an alumina PCB ready for vessel installation/calibration. c) Pd pad circuits ranging from 5-30 µm in side-length with Pt heater on top.

4: FePt

The material system selected for producing our own magnetic sensors was the binary FePt system. Like CoPtCr, FePt is heavily studied in the memory industry, specifically in the HAMR field since it has a much higher coercivity at room temperature making it difficult to rely on applied field alone to "write" data. The magnetic phase of FePt is $L1_0$ fcc phase with an easy axis along the [001] direction which is grown to have the (001) plane parallel to the sample surface. The plane orientation is formed in two main processes in literature 1) using seed layers like MgO (200) single crystal substrates so the lattice parameters between the 2 materials match up in the preferred [100] orientation, (2) growing FePt on Si/SiO_2 and use rapid thermal annealing (RTA) heating the material up to >550 °C to cause thermal expansion mismatch between FePt and SiO_2 which is minimized along the FePt (100) plane[82,83,84,85] (Figure 17). To keep most traditional CMOS and silicon microfabrication processes easily transferable, the later method of achieving the $L1_0$ FePt phase was selected.

[82] Yingguo Peng, Jian-Gang Zhu, David E. Laughlin; perpendicular thin film deposited by alternating sputtering at elevated temperature. J. Appl. Phys. 15 April 2006; 99 (8): 08F907.
[83] Jae-Song Kim, Yang-Mo Koo, Byeong-Joo Lee, Seong-Rae Lee; The origin of (001) texture evolution in FePt thin films on amorphous substrates. J. Appl. Phys. 1 March 2006; 99 (5): 053906.
[84] Albrecht, M. and Brombacher, C. (2013), Rapid thermal annealing of FePt thin films. Phys. Status Solidi A, 210: 1272-1281.
[85] Liang-Wei Wang, Wen-Chieh Shih, Yun-Chung Wu, Chih-Huang Lai; Promotion of [001]-oriented L1-FePt by rapid thermal annealing with light absorption layer. Appl. Phys. Lett. 17 December 2012; 101 (25): 252403.

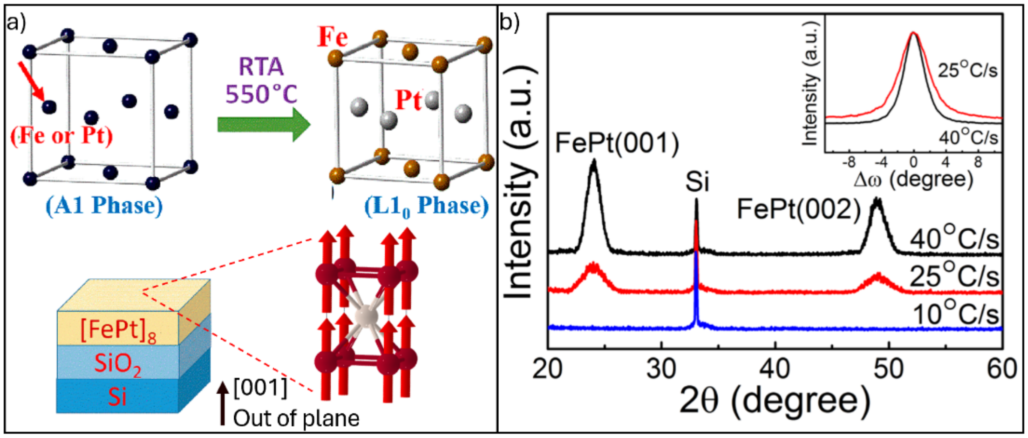

Figure 17: a) Overview of phase transition of as-deposited FePt A1 disordered phase film to $L1_0$ by thermal annealing. During this transiiton if strained properly the film will become textured to (001). b) Resulting XRD spectra for various heating rates indicating that high thermal mismatch is beneficial for FePt(001) texturing.

Having a hard magnetic material that we can deposit at any point in the fabrication process made patterning these films with either metal lift-off or reactive ion etching much easier than their CoPtCr HDD counterpart, and gave flexibility in experimental design to put the FePt sensor either on top or underneath the Pd film target.

Our standard process for producing FePt thin films with desired magnetic properties was to first use a DC-sputter target of FePt (52 at. % Fe) at room temperature in 5 mtorr Argon gas. Target power during sputtering was set to 75 W to deposit 20 nm thick films on Si (100) wafers with 3000 Å thermal SiO_2. The wafer is then thermally annealed in a RTA furnace at a ramp rate of 100 °C/s to a peak temperature of 750 °C and a hold time of 1 min in $\leq 1.0 \times 10^{-5}$ Torr vacuum. Film quality and structure was characterized using a MoK_α XRD source, AFM, EDS, and vibrating sample magnetometry (VSM). Film composition was 53 at.% Fe, 47 at.% Pt possessing similar XRD spectra (Figure 17). If annealing time is held longer than 2 min the $L1_0$ (111) peak forms indicating misorientation of the magnetic easy axis, decreasing magnetic anisotropy and therefore degrading out-of-plane properties of M_R and H_C. Surface roughness from AFM and SEM indicates average grain size to be 120 nm. A 5-10 nm thick layer of SiO_2 is coated on top of the FePt film using atomic layer deposition to protect the magnetic layer during further processing and handling.

All chip designs used this recipe for FePt synthesis and were deployed into 3 distinct experimental campaigns including NanoTI, Staring, and 400 ksi HPE femto-second laser stimulation. To enhance the coercivity for FePt, the films were etched to form isolated nanodots. This etch process formed our nanodot arrays. The physical isolation of domains from their neighbors has been shown to enhance the stability of individual single domains since the external stray fields emitted from individual neighboring domains is much lower even just a few 100 nm laterally from each dot center (Figure 18). This decreased the possibility of false positives from dot crosstalk due to strong stray fields close to the sample surface.

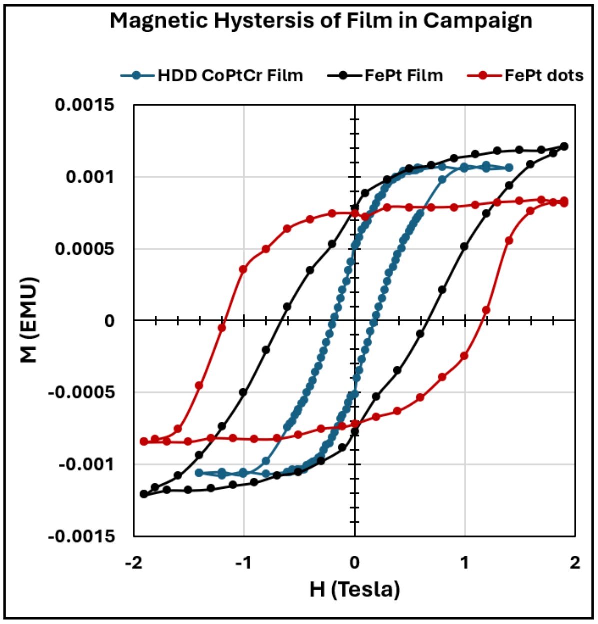

Figure 18: Magnetic Hysteresis loops collected at room temperature in nitrogen. Coercivity is enhanced for FePt after patterning to isolated nanodot length scales. Magnetization levels of FePt are slightly lower than HDD CoPtCr alloy. Film volumes kept constant with sample dimension and thickness. Dots likely have a higher M than shown.

5: **NanoTI Magnetic Archaeology Chips**

The fabrication steps for FePt sensors on NanoTI type chips are in Table 2 below. The starting substrate is Si (100) with 3000 Å SiO_2. Notice for these chips we were able to deposit the FePt layer on top of the NanoTI device (with its Pt heater and RTD) and the Pd film. The FePt dot features for this chip iteration form nano-ring-like structures which performed satisfactorily during AHE tests (Figure 19). Final chip dimensions were 5 x 7 mm.

Table 2: FePt NanoTI Fabrication Steps

Step #	Material	Method	Feature
1	5 nm Cr/ 100 nm Pt	E-beam Evap	Alignment marks
2	10 nm Cr/150 nm Au	E-beam Evap or Sputter	Interconnects/Contacts
3	100 nm SiO_2	PECVD	Passivation
4	5 nm Cr/ 50 nm Pd	E-beam Evap	Pd pads
5	5 nm Cr/ 100 nm NiCr	E-beam Evap	Pt heater/RTD
6	100 nm SiO_2	PECVD/Oxide Etcher (ICP)	Passivation/loading windows for Pd
7	20 nm FePt	DC Sputter/Positive E-beam lithography/Reactive Ion Etch	FePt 300 nm dots

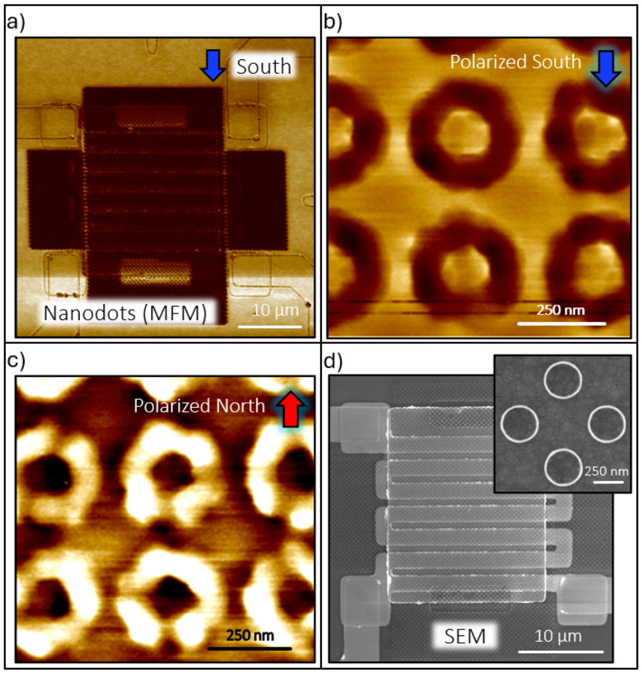

Figure 19: a) Nanodot array in preconditioned state all oriented down into the surface of the sample. b) Small area scan (1x1 µm) for dots polarized South. c) polarized North. d) SEM image of the same nanodot array, the dots are thin enough to be slightly transparent to the 10keV electron beam used to image the Pt heater. Note: these dots were processed using positive E-beam lithography leading to nanoring like strictures instead of dots, but the magnetic isolation and enhancement persisted in this morphology.

6: Staring Chips – Magnetic Archaeology

The fabrication steps for FePt sensors on Staring type chips are listed in Table 3 below. The starting substrate is Si (100) with 3000 Å SiO_2. The FePt dot sensor array is underneath the Pd for these samples. The final chip dimensions were 2x2 mm in order to fit into the 400 ksi vessel which had a bore of <0.25". With the FePt layer being annealed on a well characterized 3000 Å SiO_2 layer the remanent magnetization of these dots was more uniform than NanoTI chips allowing us to space the dots closer together and ultimately form sub 100 nm, single domain magnets for even greater spatial resolution (Figure 20). For most magnetic archaeology AHE experiments we utilized the 250 nm nanodot arrays instead of 100 nm due to having a larger stock of 250 nm generation chips (Figure 21). Aside from Staring, these chips were also used in 400 ksi experiments that stimulated the sample with a femtosecond laser.

Table 3: FePt Staring Fabrication Steps

Step #	Material	Method	Feature
1	20 nm FePt	DC Sputter/RTA 750 °C	FePt film
2	5 nm SiO2	ALD	Passivation/Resist adhesion
3	FePt	Negative E-beam lithography/Reactive Ion Etch	FePt 250 nm dots
4	FePt	RTA Anneal	Repair $L1_0$ phase
5	10 nm SiO2	PECVD	Passivation
6	5 nm Cr/ 30 nm Pd	E-beam Evap	Pd target

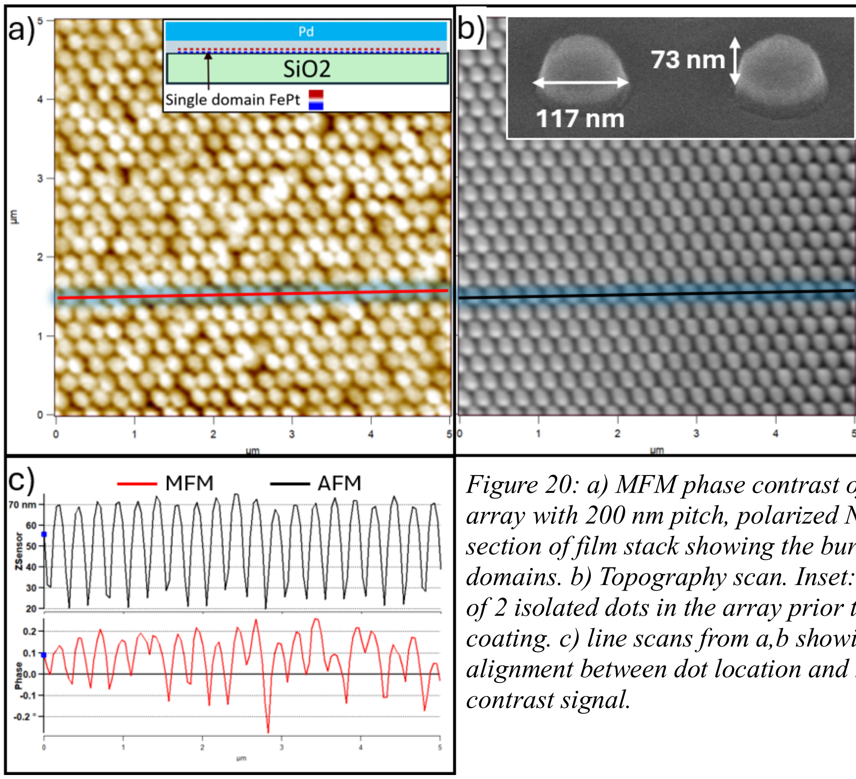

Figure 20: a) MFM phase contrast of 100 nm dot array with 200 nm pitch, polarized North. Inset: cross section of film stack showing the buried single domains. b) Topography scan. Inset: SEM tilted view of 2 isolated dots in the array prior to SiO_2 and Pd coating. c) line scans from a,b showing clear alignment between dot location and magnetic phase contrast signal.

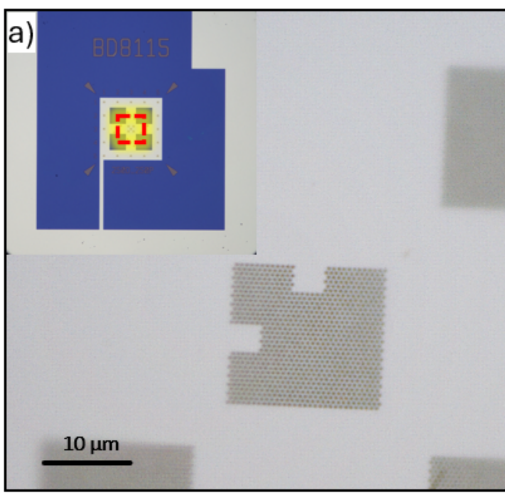

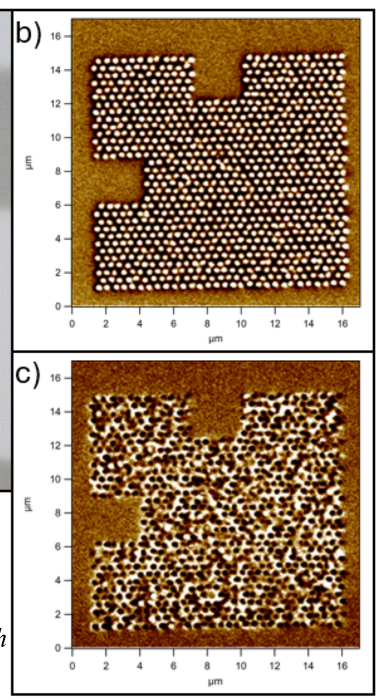

Figure 21: a) Center of BD8115, a 250 diameter by 250 nm pitch nanodot array. inset: 2x2 mm chip overview with Pd contact frame to mitigate charging issues during AFM/TMR scans. b) MFM phase contrast with North Polarization. c) South polarization.

Methods : Sample Retention

1: NanoTI-Magnetic Archaeology

The electronics used for sending and receiving electrical signals to the device are the same used in the main Chips campaign. Further details on the electronics set-up and pulse sequence is detailed in the Chips section. On top of the existing retention requirements for NanoTI chips including electrical contacts through vessel and wire-bonding, magnetic archaeology requires an applied field using a permanent magnet. This applied field was implemented using a 4 mm diameter by 2 mm thick SmCo magnet with gold plating to minimize hydrogen embrittlement of the brittle compressed SmCo powder matrix. The location of this magnet within the vessel can be seen in Figure 22. The ceramic PCB used for holding the chip in the center of the vessel is the same component used in other chip gas experiments.

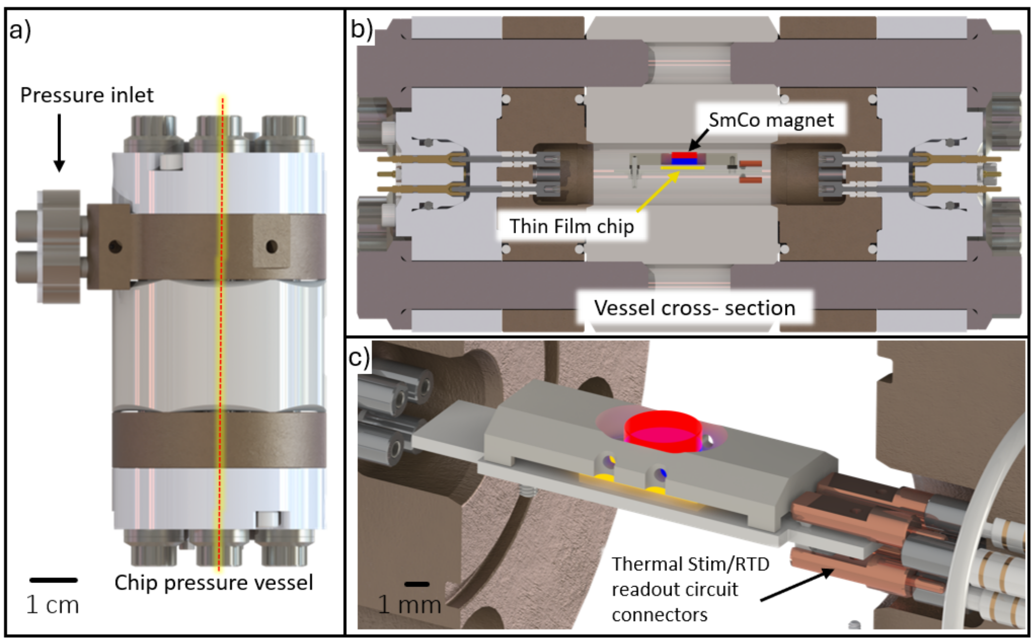

Figure 22: a) Pressure vessel overview. b) cross-section of vessel displaying locating of magnetic archaeology NanoTI PCB/chip. 2 sets of 4- pin ultrapressure feedthroughs for electrical access. C) Isometric view of chip and SmCo magnet retention with the magnet being held off the chip surface about 300 µm.

2: Staring – Magnetic Archaeology

Similar to NanoTI magnetic archaeology requirements, the sample had to be exposed to a low amplitude applied magnetic field so that when the nanodots were heated to a high enough temperature their polarity would be reoriented to the direction of the applied field prior to cooling back to room temperature. Correlating the surface temperature of the sample with a given laser profile and input power further required electrical contacts inside the pressure vessel to access the on-chip 4-wire RTD. The retention displayed in Figure 23 fulfills these retention requirements with the SmCo permanent magnet positioned behind the sample, allowing for laser access to the sample area on the front. The strength of the magnetic field at the set distance between the FePt film and the permanent magnet along the vessel axis was measured externally using a Teslameter. The field

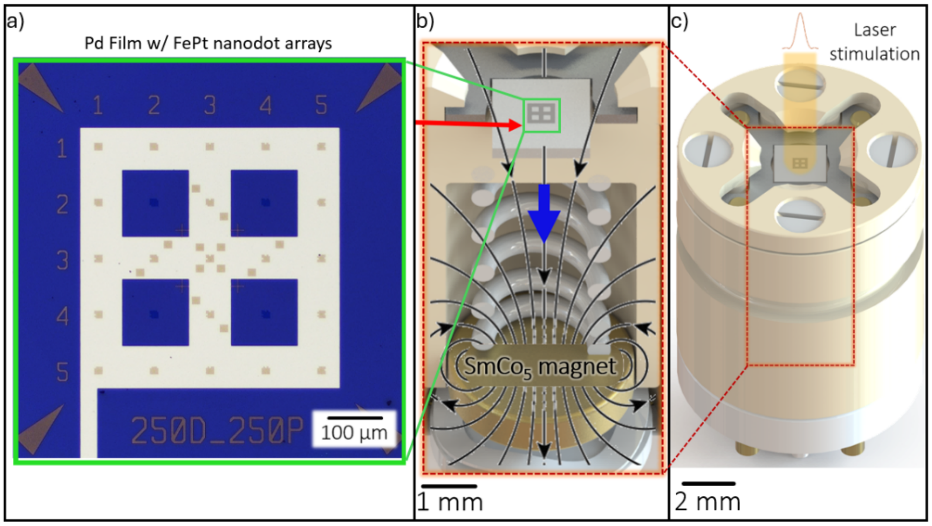

Figure 23: a) Pd window-like structure on top of >25 nanodot arrays each with 1000 dot sensors in each. b) Cross-section of sample retention for staring. The SmCo magnet is offset using a spring to reduce the field intensity at the surface of the sample to -100 mT. c) Staring sample retention with 1070 nm wavelength laser incoming from above.

amplitude was typically set to -100 mT. Further detail on the laser set-up for this and similar experiments can be found in the Staring campaign section.

3: HPE 400 ksi – Magnetic Archaeology

The 400-500 ksi pressure vessel added a tighter constraint for retaining the sample inside the vessel while keeping it properly oriented with optical access window for femtosecond laser stimulation experiments. The vessel diameter was reduced from 0.5” in 150ksi vessels to ≤ 0.25”. The solution for holding the sample and permanent magnet in place during the duration of the experiment, without damage to the sample during install or removal is detailed in USP and HPE sections of this report. In short, a set of countersunk Toughmet retaining rings hold the 2x2 mm chip loosely along the optical axis. A compression spring presses all surfaces of the Toughmet ring, sapphire window, and permanent magnet gently into one another so the retention remains in place prior to press-up to 400 ksi and beyond.

Results

Utilizing these submicron magnetic sensors as heat detectors produced experimental results that were reproducible between various campaigns leading the same general result of observing no indication of local thermal events within the Pd film. We can also have high confidence that the magnetic sensors deployed for this AHE search should be sensitive to a single 24 MeV event.

These results are covered in further detail in the subsections below moving from magnetic material stability testing for both HDD and FePt systems to full pressure stimulation experiments in both protium and deuterium for NanoTI, Staring, and 400 ksi HPE vessel campaigns.

Results : Ultrapressure gas degradation tests

HDD films, FePt films, and FePt nanodots were subjected to deuterium gas up to 400 ksi. All films were coated with 10 nm PECVD SiO_2 as a protective layer. The films were left under this deuterium and protium environment for 1 hour prior to removal and post characterization with MFM. No obvious changes to magnetic polarity could be measured using MFM, and magnetic hysteresis loops of films exposed to hydrogen showed no significant changes in coercivity and magnetization (Figure 24).

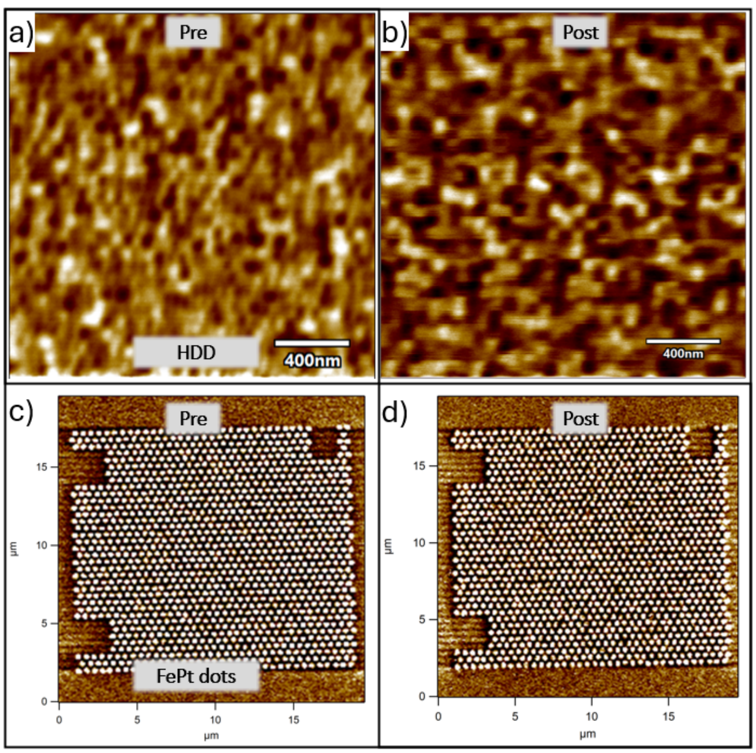

Figure 24: a, b) HDD, CoPtCr media before exposure to ultrapressure hydrogen and after showing the magnetic domain structure is retained. c, d) MFM scan of FePt nanodot array showing the magnet domain strucutre is retained after ultrapressure testing.

Results : Confirmation of ultrafast switching of domains

To confirm that both HDD and FePt type magnetic sensors could record nuclear events that may occur as fast as the picosecond timescale, a series of experiments were completed that used a femtosecond 450 nm laser to locally pump energy into the Staring and NanoTI type film stacks within an area of 10-30 µm in diameter. The pulse width for all tests was on average 40 fs with a rep-rate of 1-5 Hz. The excitation fluence for each pulse was increased between 0.01- 10 µJ/cm^2, spanning the range from below domain reversal threshold to above film damage threshold. An external applied field with an amplitude of 150 mT was applied perpendicular to the sample surface to reverse domains that have become destabilized from local heating within the laser spot. For HDD devices the fluence level for domain reversal was roughly 0.60 µJ/cm^2, and FePt devices 1.1 µJ/cm^2 (Figure 25). These results confirm the magnetic materials used can record a local thermal stimulus, over fsec-psec timescales, in the magnetic domain polarity of the film. This is fundamental in HAMR and ultrafast optical switching; however, it was imperative to confirm this effect with the films being used as AHE detectors[86,87.]

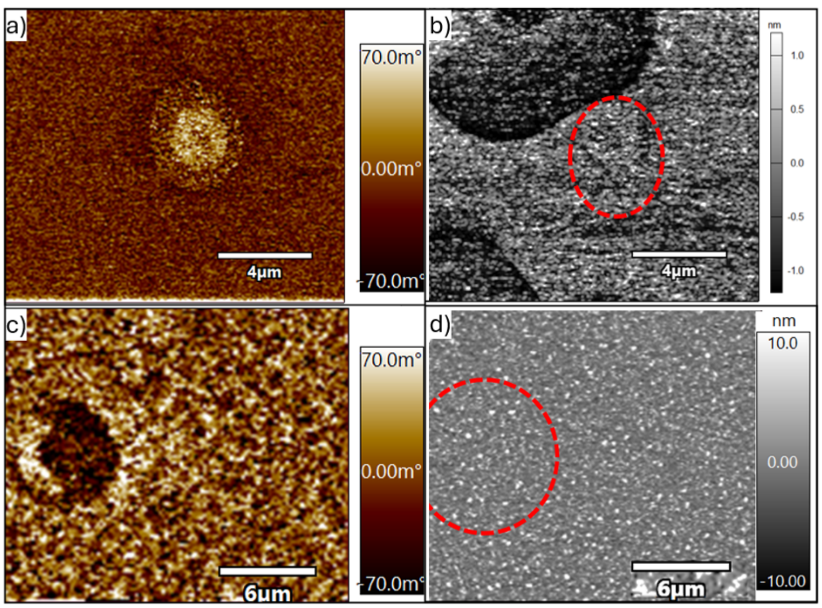

Figure 25: a) MFM phase contrast of CoPtCr magnetic HDD film showing clear domain structure change where the femtosecond laser impinged on the surface. b) Same scan area as a) showing topography, no physical damaged manifested within laser spot (red). c) MFM phase contrast of FePt film showing clear domain structure change (in presence of a South oriented H_{ext}) where the femtosecond laser impinged on the surface. d) No physical damage observed in the same location shown in c).

Results : Single Event Detection Simulation

Based off published values for FePt, hydrogen gas, and CMOS based chip architectures, a thermal simulation using COMSOL Multiphysics was performed to help quantify our AHE sensitivity

---

[86] Kelvin Yao, Felix Steinbach, Martin Borchert, Daniel Schick, Dieter Engel, Filippo Bencivenga, Riccardo Mincigrucci, Laura Foglia, Emanuele Pedersoli, Dario De Angelis, Matteo Pancaldi, Björn Wehinger, Flavio Capotondi, Claudio Masciovecchio, Stefan Eisebitt, and Clemens von Korff Schmising. *Nano Letters* **2022** *22* (11), 4452-4458.

[87] Xie Z, Cai Y, Tang M, Zhou J, Liu J, Peng J, Jiang T, Shi Z, Chen Z. Fluence and Temperature Dependences of Laser-Induced Ultrafast Demagnetization and Recovery Dynamics in *L*1_0-FePt Thin Film. *Materials*. 2023; 16(14):5086.

using this magnetic detection method[88,89]. Accounting for convection and conduction coefficients and using a 24 MeV heat source as the thermal input to the system, we defined the radial sensitivity of a single 250 nm FePt dot from its center. To reduce model complexity this simulation only models heat transfer in 3D with thin film approximation. The change in magnetic properties based off the thermal input was not modeled, and instead a threshold temperature of 300 °C was defined, above which it is assumed the nanodot single domain would destabilize and flip in the applied field direction. Other assumptions made for this model are 1) a 20 ps pulse width over which the 24 MeV event would be released and 2) the event sphere has a radius of 2 nm over which the energy will be emitted from. Figure 26 shows the 3D representation of this film stack and the change in

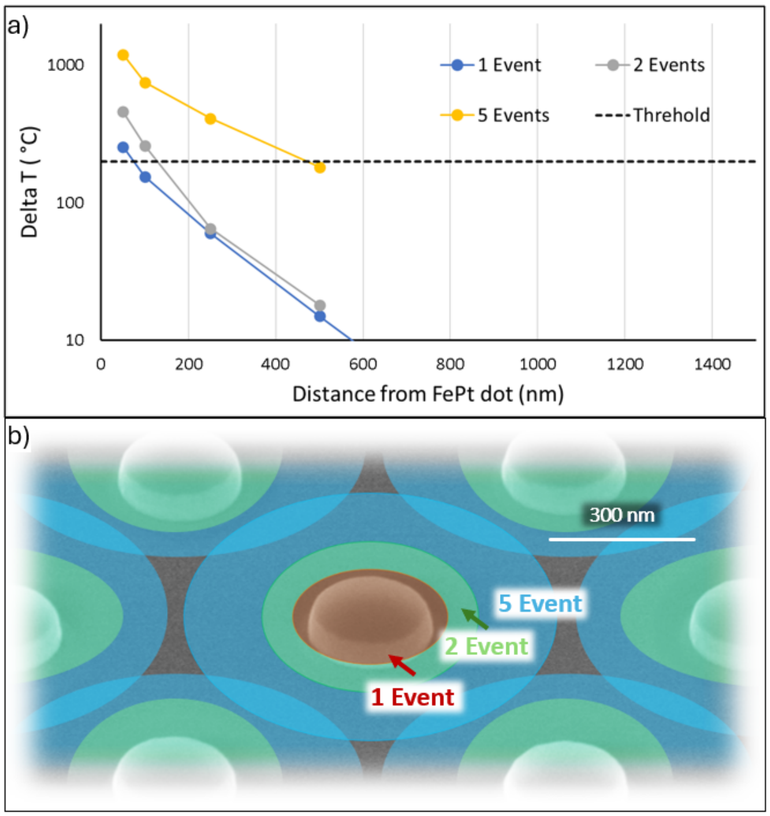

Figure 26: a) Temperature change vs. lateral distance from dot center as a function of 24 MeV AHE events. b) Tilted SEM view of FePt nanodot array with overlayed sensitivity color map.

temperature as a function of radial distance from dot center and number of events occurring within 20 ps. Through this basic heat transfer model, we can have a level of confidence that we have single event sensitivity within 100-200 nm from the center of a 250 nm nanodot. Within the 250 nm nanodot array with 500 nm pitch from center to center, 1-5 AHE events should be detectable using this magnetic recording approach.

---

[88] S. E. Russek and W. E. Bailey, "Magnetic domain structure and imaging of Co-Pt multilayer thin-film nanostructures," in *IEEE Transactions on Magnetics*, vol. 36, no. 5, pp. 2990-2992, Sept 2000.
[89] H. Z. Yang, Y. J. Chen, S. H. Leong, C. W. An, K. D. Ye, M. J. Yin, J. F. Hu; A multi-functional testing instrument for heat assisted magnetic recording media. *J. Appl. Phys.* 7 May 2014.

Results : Magnetic Archaeology – NanoTI FePt dots (300 nm)

The thermal stimulation applied for these experiments was the same used in all other NanoTI chip campaigns. Further detail on experimental design of the electrical circuit can be found in the Chips section. With a stimulation pulse width of 10 μs and varying the voltage between 1-6 V the heater circuit was able to heat up to 350 °C without thermally degrading the circuit (Figure 27). Running 3-4 samples in deuterium at 145 ksi we did not observe domains reversal from the preconditioned state of south when heating below 325 °C. The MFM contrast clearly indicates there is no individual sensor being flipped to the applied field direction of north (Figure 28). With these stimulation conditions no observable AHE events could be confirmed.

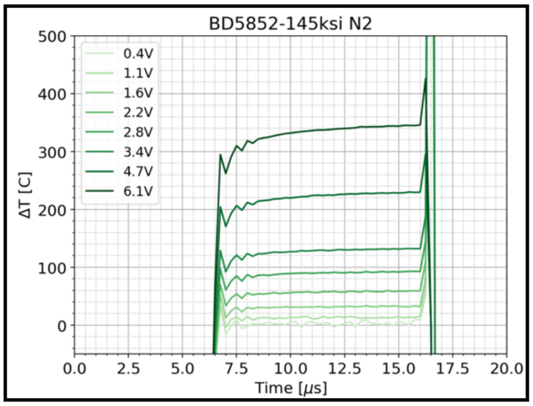

Figure 27:Resulting temperature increase of the Pt heater circuit as a function of input voltage with constant current. We can stimulate above and below any Curie Temperature the films may possess.

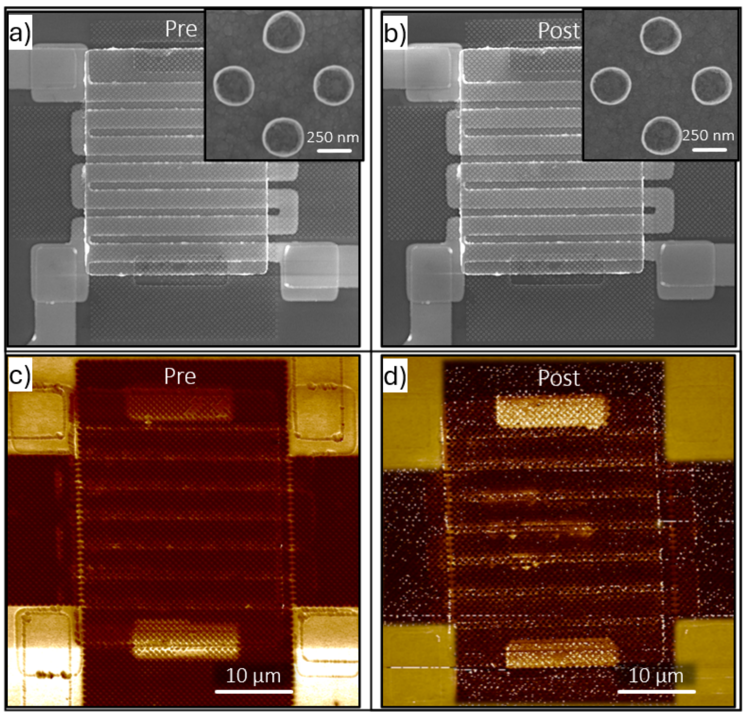

Figure 28: a) Pre SEM image of NanoTI with FePt nanodot sensors on top. b) post SEM showing no obvious signs of damage. c,d) Pre/Post MFM showing no signs of domain reversal from south to North.

These chips proved to be difficult to reproduce between wafer batches due to variations in the PECVD SiO_2 layer that supported the FePt dots. Furthermore, with the Pt heater underneath the FePt, this Pt heater needed to be processed during fabrication through rapid temperature changes up to 750 °C, which unfortunately can change the resistance of the Pt heater circuit leading to variation in our thermal calibrations as well. This variation leads to large uncertainties (50-100 °C) in how hot we are heating our Pd and FePt sensors. With this in mind, the remainder of magnetic archaeology stimulation was focused on laser-based heating using the 1070 nm and femtosecond 450 nm wavelengths.

1: HDD/CoPtCr Sensors

To not damage our CoPtCr sensors, temperature calibrations were completed using an on chip RTD to measure the peak average surface temperature of a 750 µm diameter 1070 nm laser spot (Figure 29a). This calibration located the damage threshold and switching threshold powers for the CoPtCr film. The damage threshold measured to be >18 W, while the domain switching threshold, regardless of the applied field, was between 16-17 W (Figure 29b,c). AHE experiments were carried out in both 145 ksi protium and deuterium with input power set to 16 W. Neither condition produced reliable domain reversal in the stimulated laser spot region. Ultimately the fact these HDD films were continuous in nature with little space between domains, made it exceedingly difficult to interpret the MFM contrast scans between pre and post. Neighboring domains would

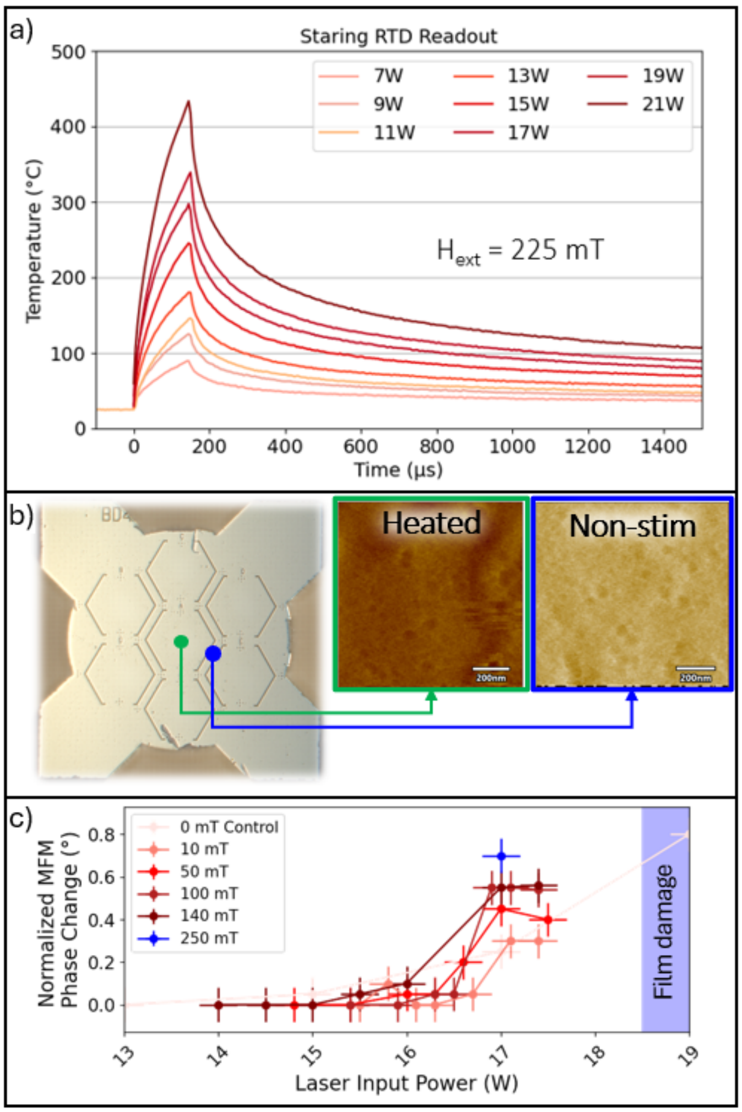

Figure 29: a) RTD calibration temperature profiles for each laser input condition. b) Method used to measure changes in MFM phase contrast, subtracting out background (blue) from the stimulated region (green). c) Phase contrast normalized to a complete domain reversal (=1). There is a slight trend of decreased power required for increasing Hext, but not significant enough to be controllable under these extreme environments.

flip others stochastically. For this reason, we moved quicky to FePt based sensors where we obtained much better stability and reproducibility.

2: FePt dots (250 nm)

The FePt nanodot with Pd films were exposed to 150 ksi deuterium and protium gases while being stimulated with a 1070 nm wavelength laser at various input power conditions and pulse lengths. The beam diameter was 1 mm, and a calibration RTD chip with the same film stack as our actual magnetic sensor samples was used to calculate how hot the surface of the Pd was during laser heating. Knowing the peak temperature of the film is critical because there is a maximum service temperature that FePt films can operate at without completely destabilizing and that is the Curie Temperature (T_C). This calibration ensures the laser parameters on our Pd/FePt samples will keep the peak temperature well below T_C to ensure we do not get false positives from laser stimulation alone. The calibration results can be found in Figure 30 where we heated the calibration chip up to 600 °C. For all Staring tests we aimed to keep the film temperature at or below 300°C so we remain well below the average T_C of 450°C and variability around this temperature up to 50 °C in bulk films based off possible local variability in phase structure, composition, finite size effects[90,91,92].

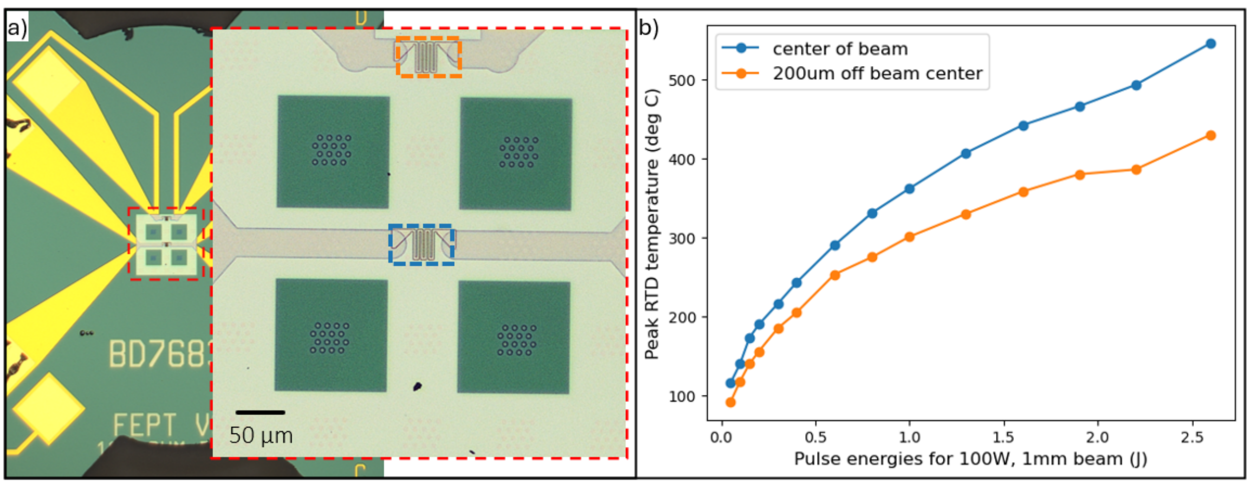

Figure 30: a) Calibration RTD chip with 2 4-wire RTD circuits with 1 mm diameter beam, inset: center of chip with serpentine Pt RTDs. b) Peak temperature values for each pulse of 100 W at varying pulse lengths between 1-70 ms.

A total of 10 individual Pd/FePt samples were loaded and thermally stimulated in the Staring apparatus, 5 deuterium and 5 protium. All samples that were heated up to a peak temperature of 300 °C or below showed no indication of AHE. Clean PdH_x and PdD_x samples showed no clear

---

[90] L Rohman *et al* 2020 *J. Phys.: Conf. Ser.* **1491** 01 2013.

[91] Nguyen Thanh Binh, Sergiu Ruta, Ondrej Hovorka, Richard F. L. Evans, and Roy W. Chantrell, Phys. Rev. B 106, 054421 – Published 17 August 2022

[92] Bublat, T. & Goll, D.. (2010). Temperature dependence of the magnetic properties of L10-FePt nanostructures and films. Journal of Applied Physics. 108.

changes in magnetic polarity when scanned using MFM after stimulation. All domains remained oriented in the northward direction out-of-plane (Figure 31). With this result there were no indications that the Pd film heated up locally due to AHE activity.

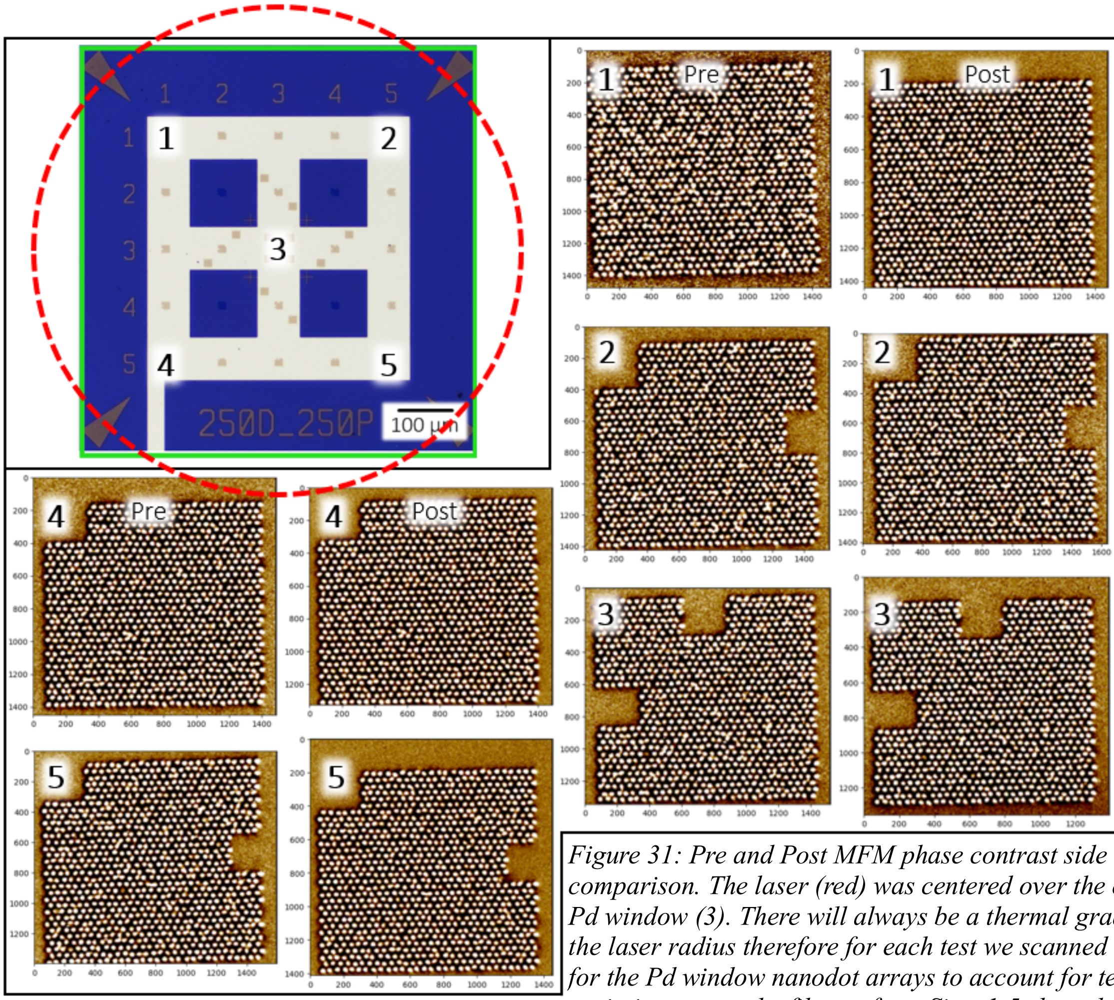

Figure 31: Pre and Post MFM phase contrast side by side comparison. The laser (red) was centered over the center of the Pd window (3). There will always be a thermal gradient along the laser radius therefore for each test we scanned the 4 corners for the Pd window nanodot arrays to account for temperature variation across the film surface. Sites 1-5 show the raw MFM phase scans where all domains remain polarized in the preconditioned orientation, North.

There were sources of contamination that could cause a false positive in our MFM readout. This contamination mainly formed through initial poor sample handling practice and powerpack inlet line particulate adhering to the surface of the sample. If a carbon-based contamination or particle with increased roughness is locally covering some of the FePt nanodots, there is increased absorbance in those locations leading to higher peak temperatures locally within a nanodot array. These false positives are caught by collecting overview SEM images of each nanodot array after a pressure test is completed (Figure 32). This contamination effect occurred in the femtosecond laser experiments as well and was accounted for in final conclusions for this study.

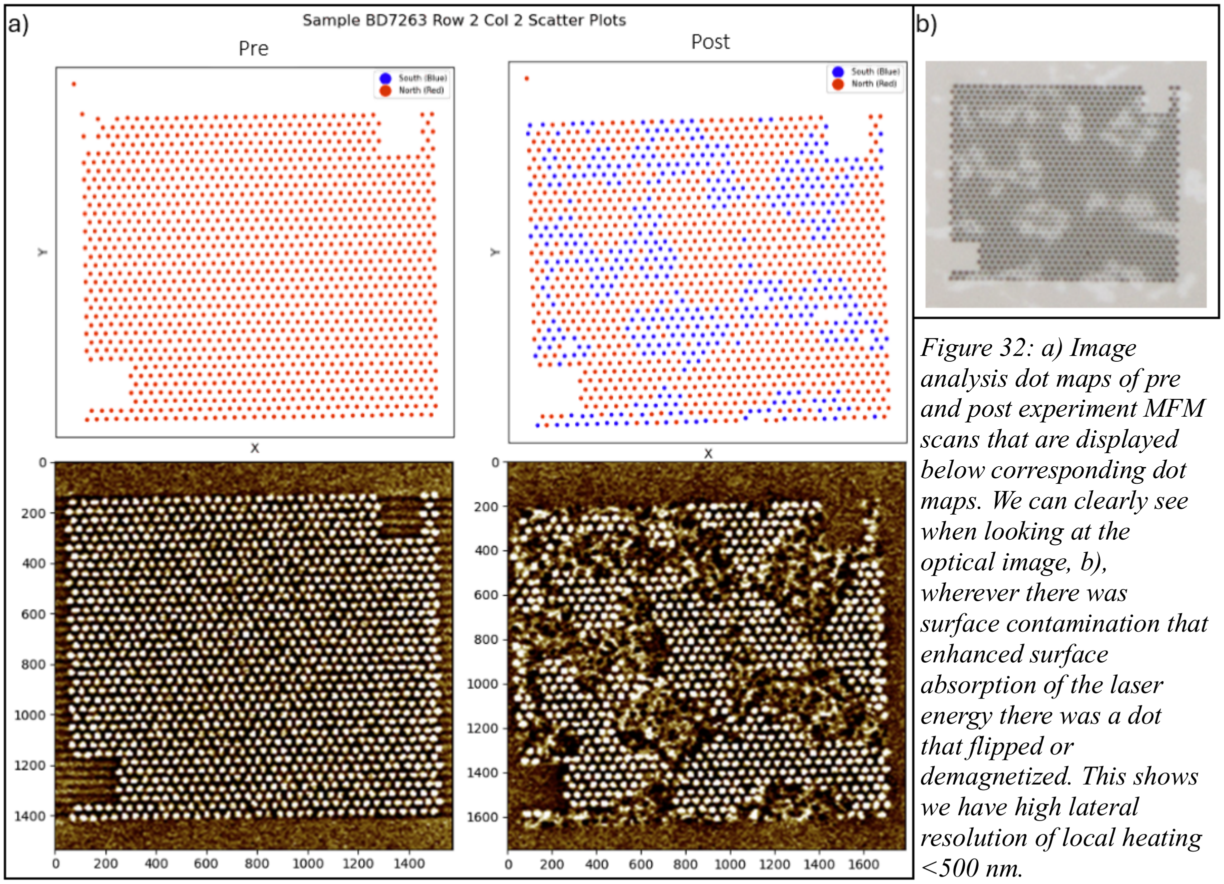

Figure 32: a) Image analysis dot maps of pre and post experiment MFM scans that are displayed below corresponding dot maps. We can clearly see when looking at the optical image, b), wherever there was surface contamination that enhanced surface absorption of the laser energy there was a dot that flipped or demagnetized. This shows we have high lateral resolution of local heating <500 nm.

Results : Magnetic Archaeology : 400 ksi, femtosecond laser

Exposing the Pd/FePt nanodot array chips to 400 ksi ensured maximum deuteron and proton loading prior to stimulation using a 450 nm femtosecond laser. For these experiments laser parameters were selected based off damage threshold and domain reversal threshold calibration studies where the beam diameter was focused to 150 µm and pulse width <100 fs. If we saw no domains flip in either protium or deuterium at a given input energy level, the temperature reached locally around each nanodot is known to be below the domain reversal temperature (T_S). Directly measuring the film temperature in a 400 ksi gas environment and at these ultrafast timescales was not feasible at the time of this study. A total of 8 thermal stimulation tests were completed with laser parameters that stimulated the sample below T_S, 6 in deuterium and 2 in protium as controls. Figure 33 shows multiple nanodot arrays at various locations around the center of the sample. All five locations show no clear changes in domain polarity from north indicating no hot spots were detected in those locations before, during, or after laser stimulation. Table 4 lists the entirety of all AHE experiments the various magnetic sensors were utilized for heat detection.

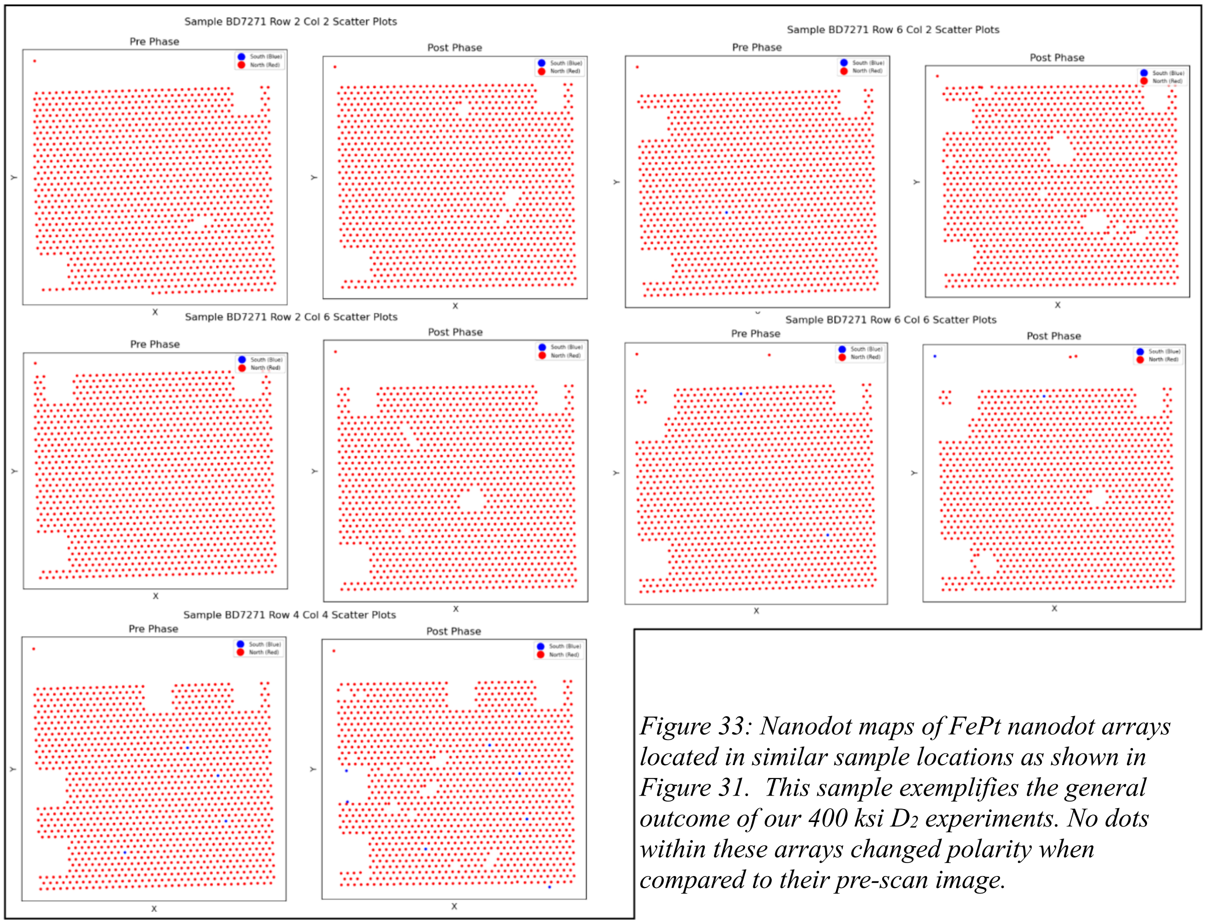

Figure 33: Nanodot maps of FePt nanodot arrays located in similar sample locations as shown in Figure 31. This sample exemplifies the general outcome of our 400 ksi D_2 experiments. No dots within these arrays changed polarity when compared to their pre-scan image.

*Table 4: AHE Experiments using Magnetic Sensor**

NanoTI				
BE	Sample type	Gas	Pressure (ksi)	Peak Temperature (°C)
2351	HDD/CoPtCr	N2	120	350
2442	HDD/CoPtCr	D2	140	450
2518	HDD/CoPtCr	H2	140	450
2621	HDD/CoPtCr	H2	140	450
3297	HDD/CoPtCr	D2	100	300
3318	FePt 300 nm dots	D2	100	300
Staring				
BE	Sample type	Gas	Pressure (ksi)	Peak Power (W) / Temperature
1845	HDD/CoPtCr	D2	145	19.2
1936	HDD/CoPtCr	D2	145	19.2
2059	HDD/CoPtCr	D2	145	23
2290	HDD/CoPtCr	D2	145	17
2519	HDD/CoPtCr	H2	120	17

2532	HDD/CoPtCr	H2	145	17
2710	HDD/CoPtCr	D2	140	15
2722	HDD/CoPtCr	D2	145	15
2732	HDD/CoPtCr	D2	145	15
2739	HDD/CoPtCr	D2	140	15
3611	FePt 300 nm dots	D2	150	11
3715	FePt 300 nm dots	D2	140	13/300 °C
3738	FePt 300 nm dots	D2	140	12/250 °C
3778	FePt 300 nm dots	D2	140	12/250 °C
3824	FePt 300 nm dots	D2	145	No Stim
3990	FePt 300 nm dots	D2	145	300 °C
4013	FePt 300 nm dots	D2	145	250 °C
4045	FePt 250 nm dots	D2	140	250 °C
4058	FePt 250 nm dots	H2	145	250 °C
4063	FePt 250 nm dots	H2	145	250 °C
4093	FePt 250 nm dots	D2	145	250 °C
4097	FePt 250 nm dots	D2	145	200 °C
4101	FePt 250 nm dots	H2	145	200 °C
4121	FePt 250 nm dots	D2	145	250 °C
4123	FePt 250 nm dots	H2	140	250 °C
4144	FePt 250 nm dots	H2	140	50 °C
4189	FePt 250 nm dots	D2	140	50 °C
4190	FePt 250 nm dots	D2	140	250 °C
400 ksi femtosecond laser				
BE	Sample type	Gas	Pressure (ksi)	Peak Power (W)**
3899	FePt 250 nm dots	D2	400	No Stim
3906	FePt 250 nm dots	H2	400	75 %
3941	FePt 250 nm dots	H2	400	60 %
3964	FePt 250 nm dots	H2	400	30 %
3978	FePt 250 nm dots	H2	400	15 %
4022	FePt 250 nm dots	H2	400	7.5 %
4057	FePt 250 nm dots	D2	400	7.5 %

*The BEs in this table are only experiments that were clean AHE tests, these are not including calibrations, optimization experiments, pressure test, offline stim testing, and most inert gas tests.
**Peak power value is based of % of full power of femtosecond laser upstream from pressure vessel, refer to USP for values and further details

Conclusion

Reflecting back, LENR is believed to produce local hot spots that form and dissipate quickly, only affecting a small volume (~ 100 nm in size) for a very short time (~ 1 psec). The extreme difficulty of detecting temperature pulses with both this temporal and this spatial resolution was the reason for developing the various magnetic heat sensors discussed in this section. Throughout our suite of experiments, we have confirmed that the sensors fabricated can respond to ultrafast energy pulses at the local <1 μm length scales in proximity to a PdD_x lattice. With the single event sensitivity achieved for Pd thin film-based samples, we have not observed AHE production at the various pressure, temperature, and loading conditions probed in this study.